US 2020260697A1

(54) **METHODS OF MOUSE CLINICAL TRIAL**

(71) Applicant: **CROWN BIOSCIENCE, INC. (TAICANG)**, Taicang, Jiangsu (CN)

(72) Inventors: **Sheng GUO**, Taicang (CN); **Henry Qixiang LI**, Oceanside, CA (US)
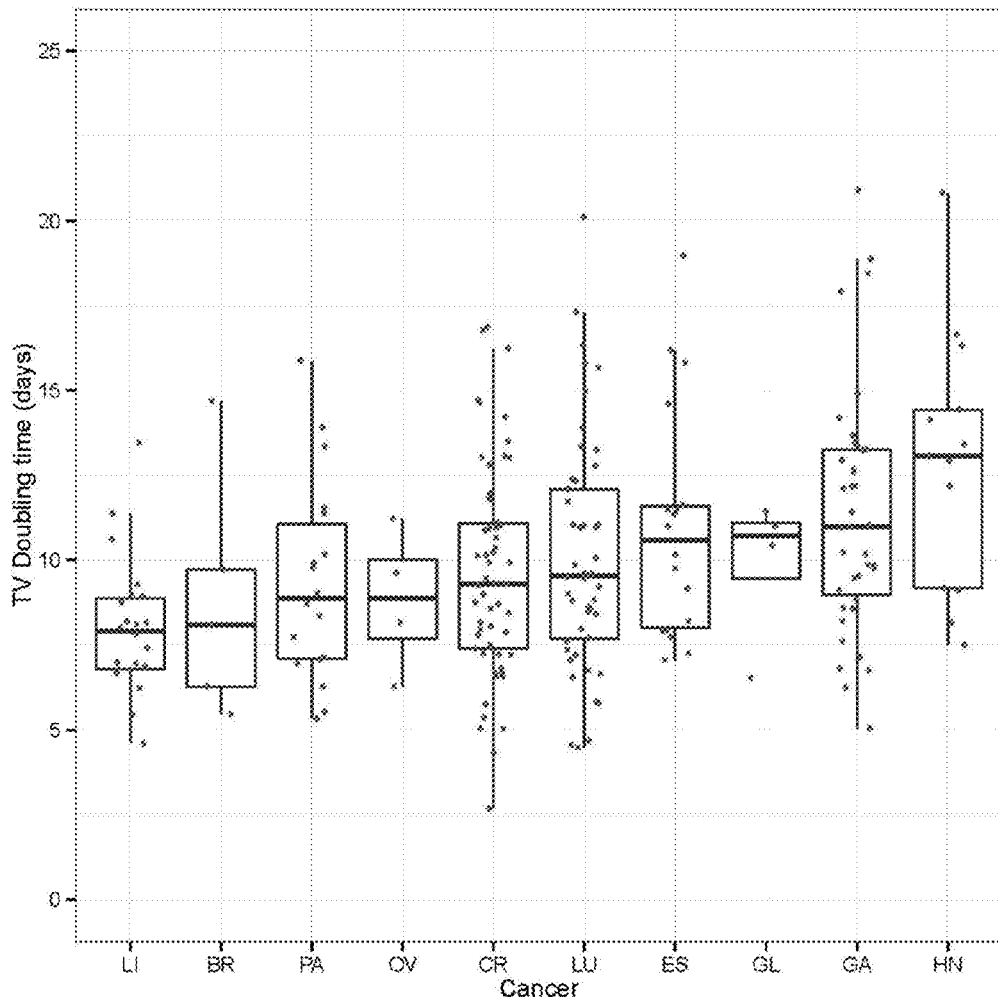
(57) **ABSTRACT**

The present disclosure provides methods of conducting and analyzing mouse clinical trials. In one embodiment, the method comprises the steps of receiving a dataset of tumor volumes measured in a mouse clinical trial, determining tumor growth curve of the treatment group and tumor growth curve of the control group; determining area under curve (AUC) of the treatment group and AUC of the control group; and evaluating efficacy of the drug based on an AUC ratio between the AUC of the treatment group and the AUC of the control group, wherein the mouse clinical trial comprises the steps of: obtaining a tumor sample derived from a patient; grafting the tumor sample to a treatment group comprising m mice and a control group comprising n mice, wherein m and n are integers; treating the treatment group with a drug; treating the control group with a vehicle; and measuring tumor volume of the treatment group and tumor volume of the control group at a plurality of days.
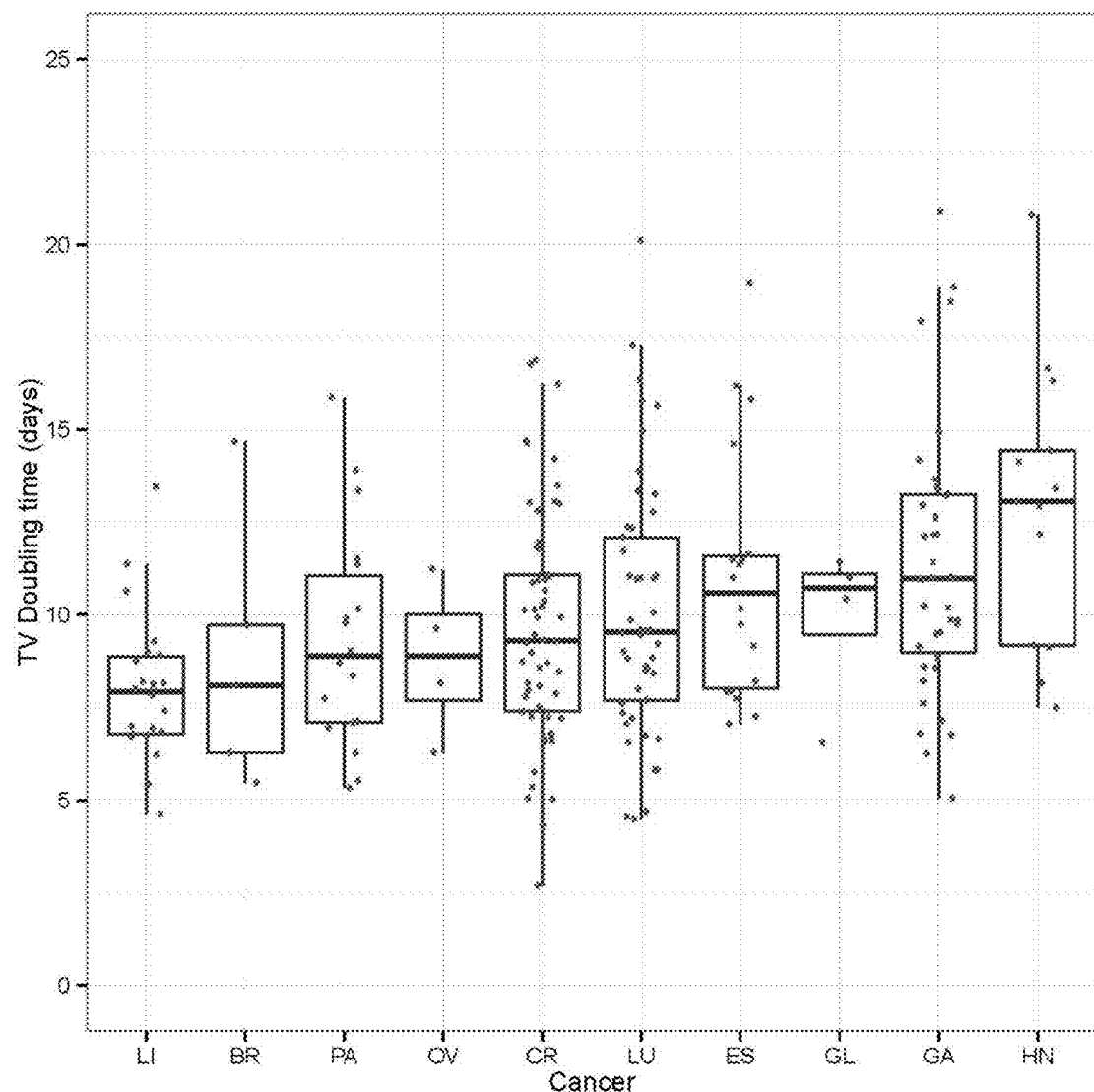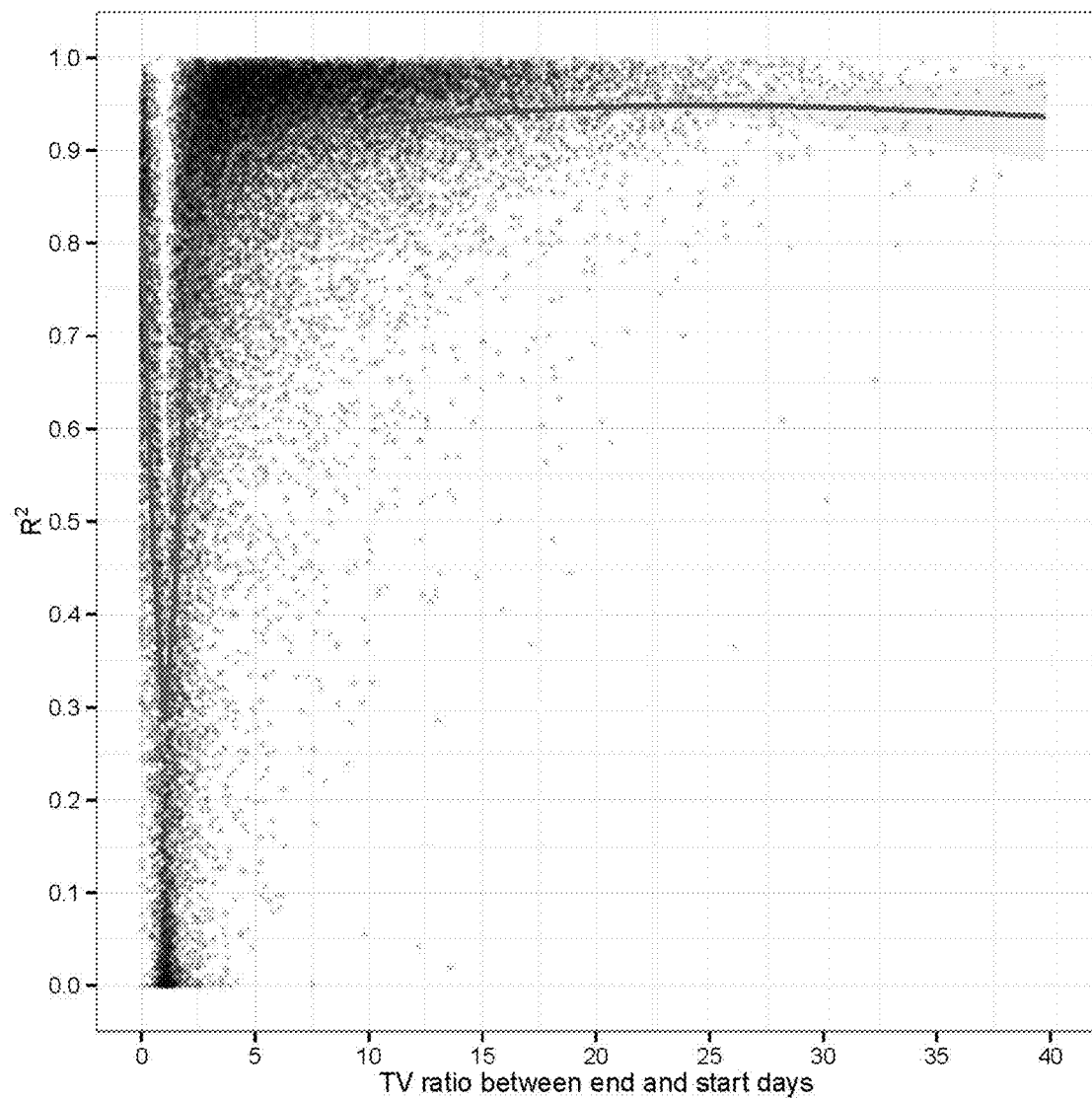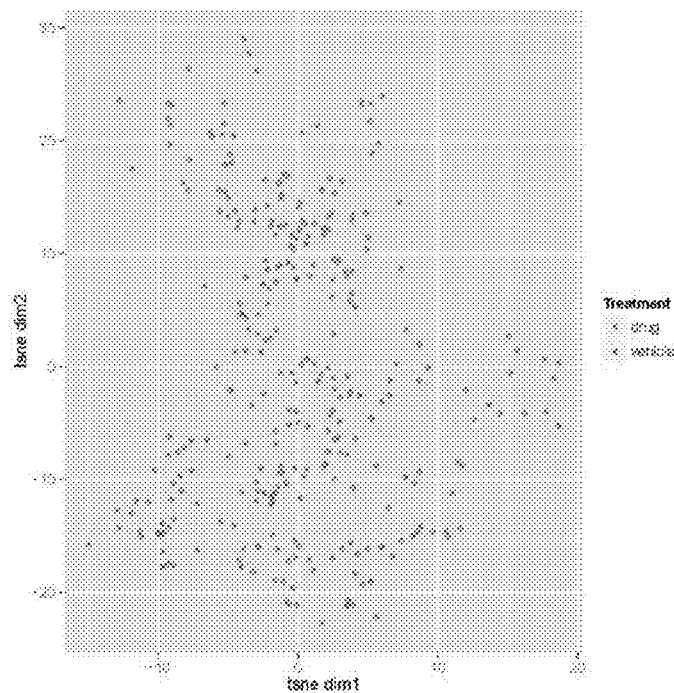
Figure 1

Figure 2

Figure 3A
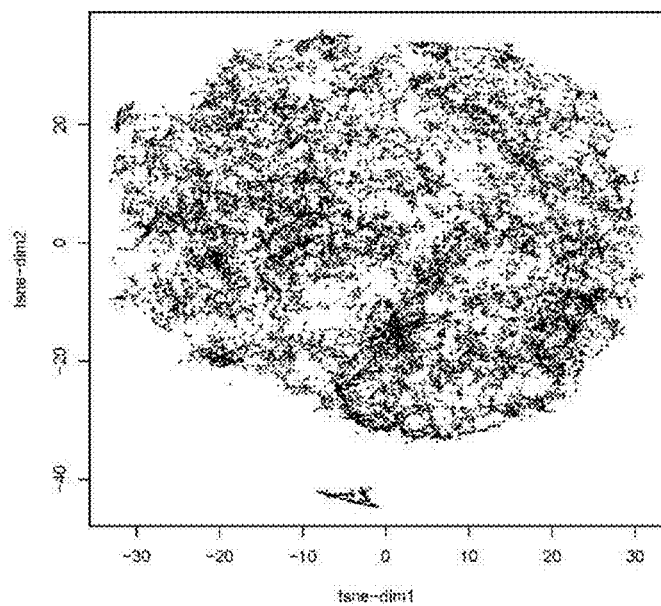
Figure 3B
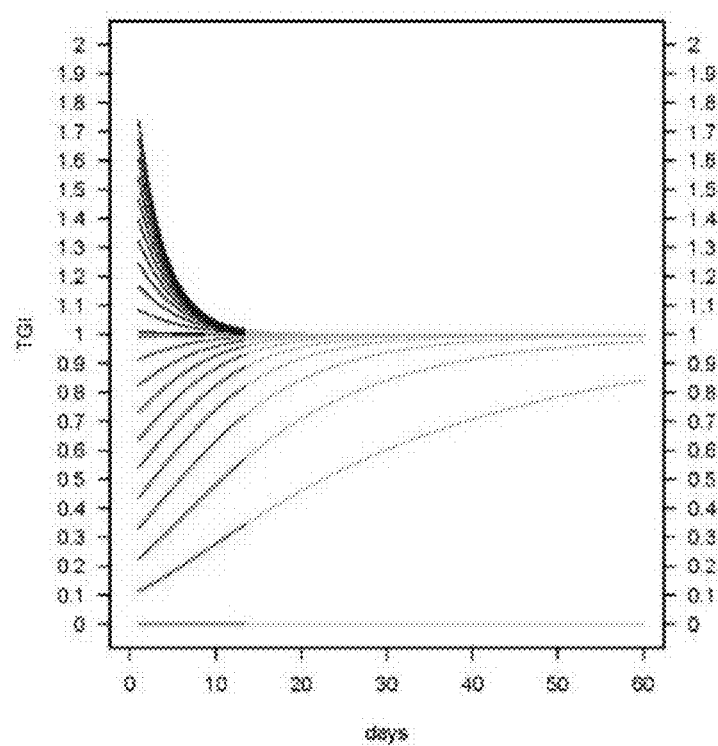
Figure 4A
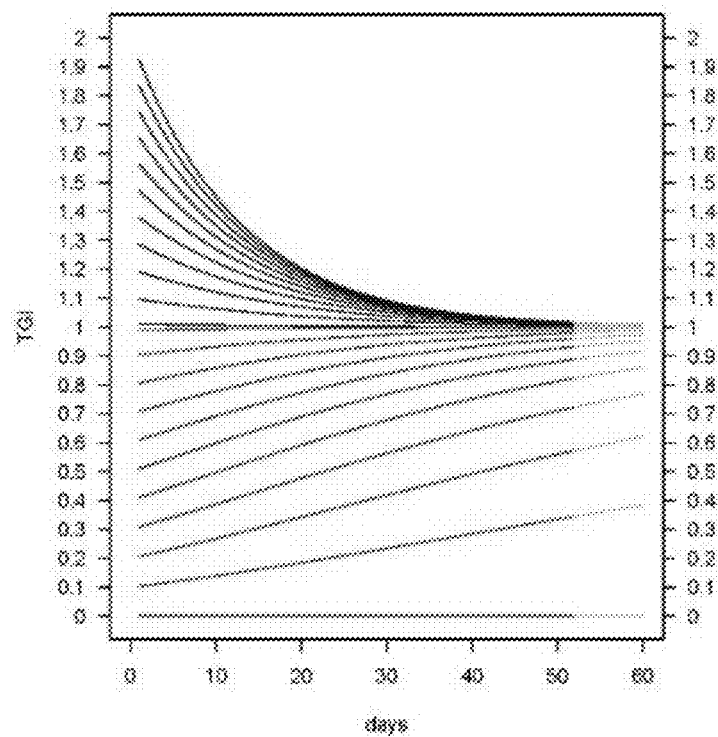
Figure 4B
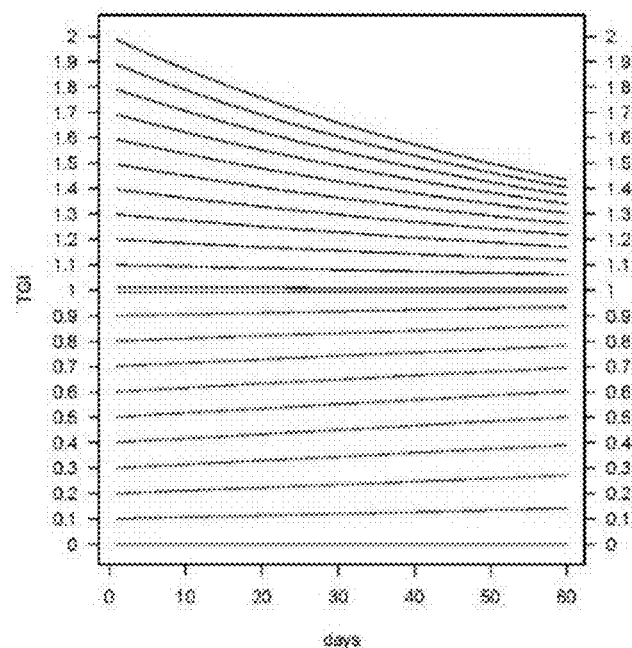
Figure 4C
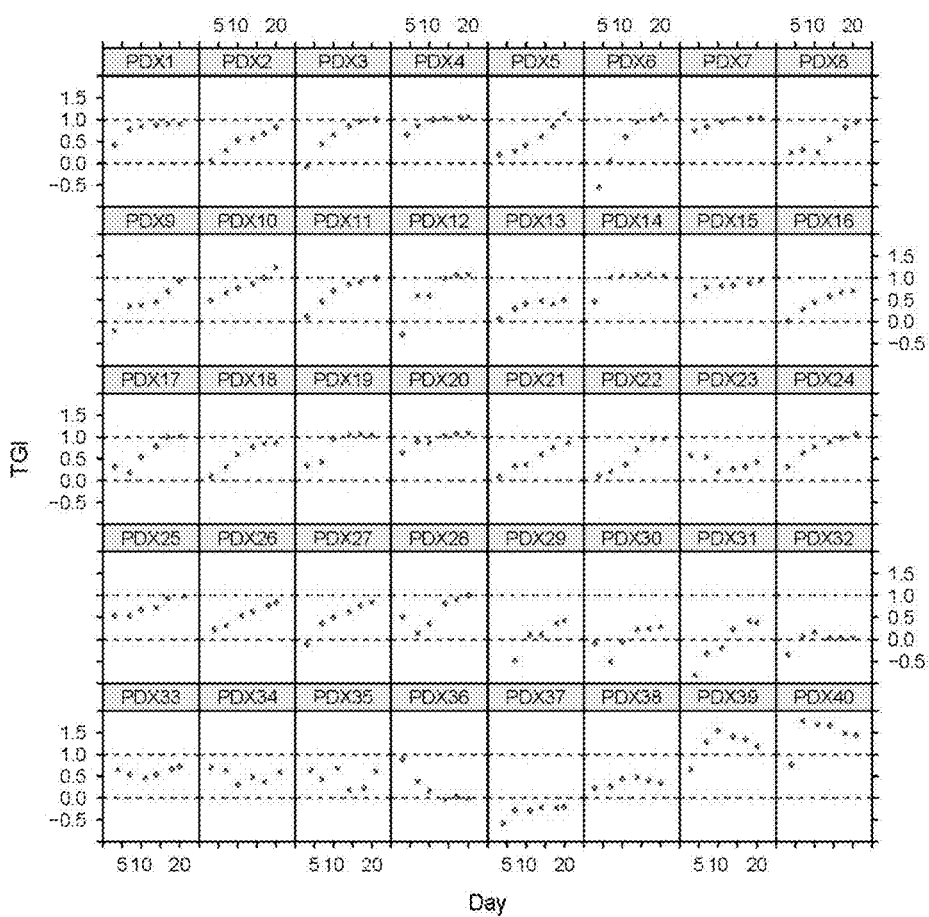
Figure 5A
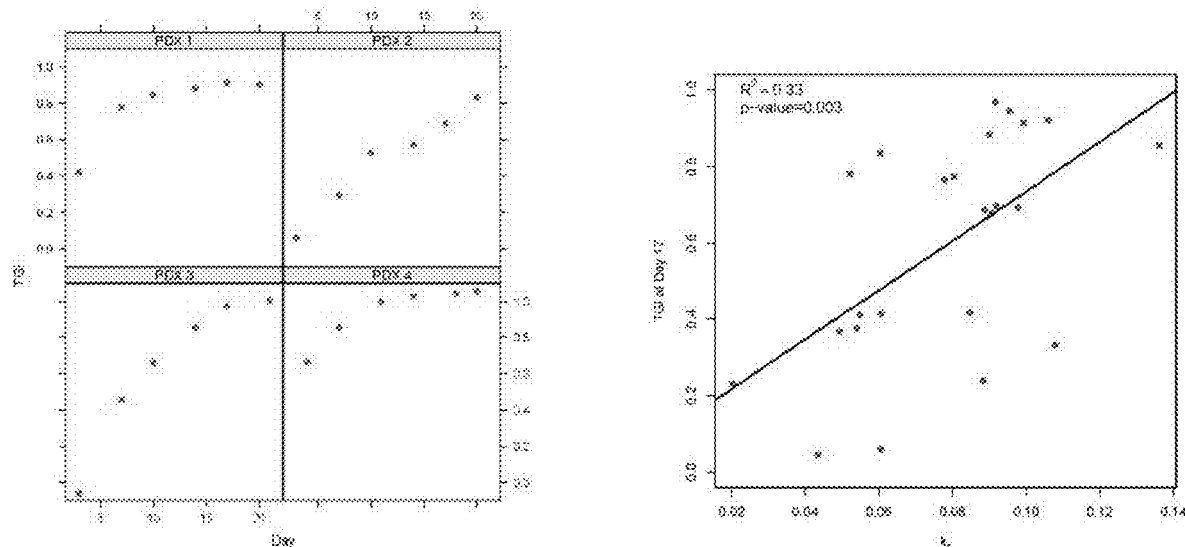
Figure 5B
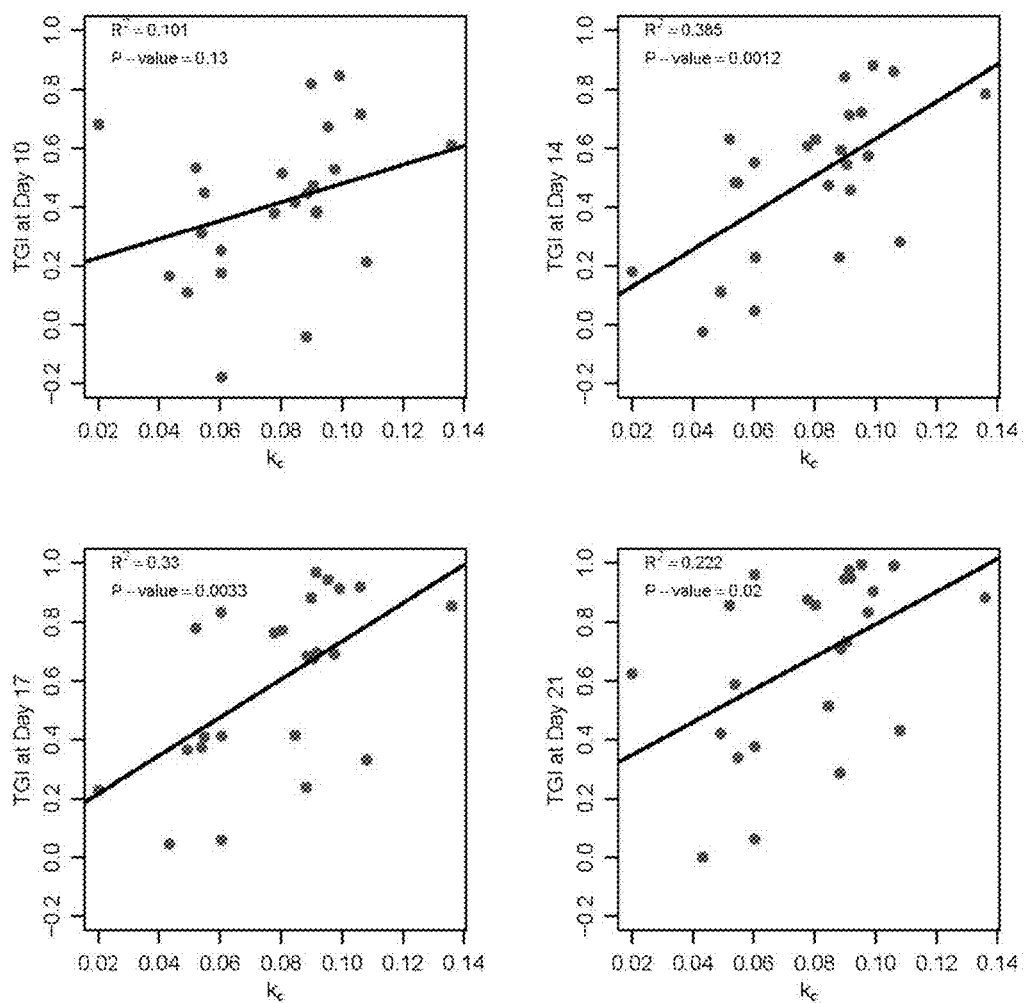
Figure 5C
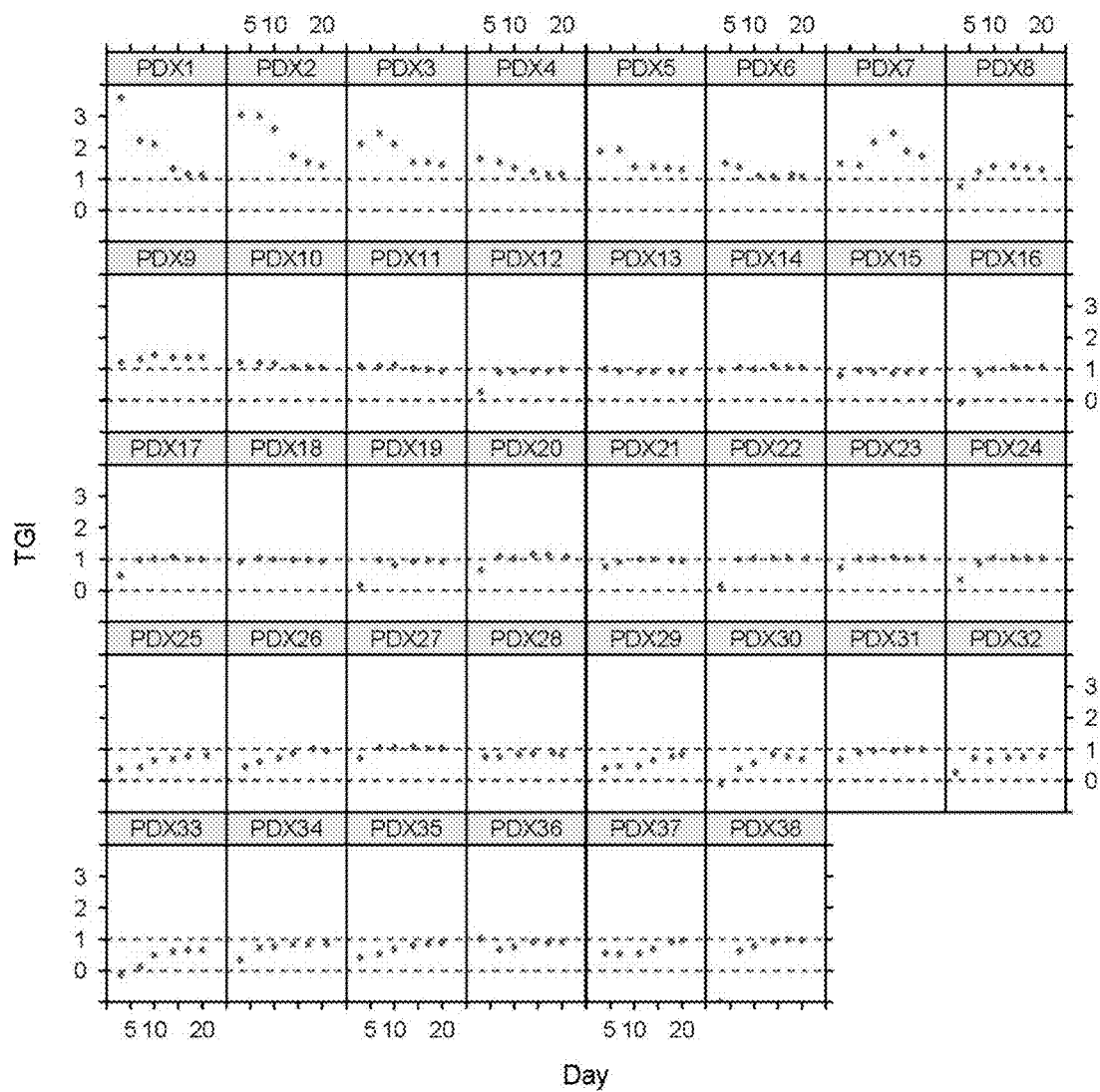
Figure 5D
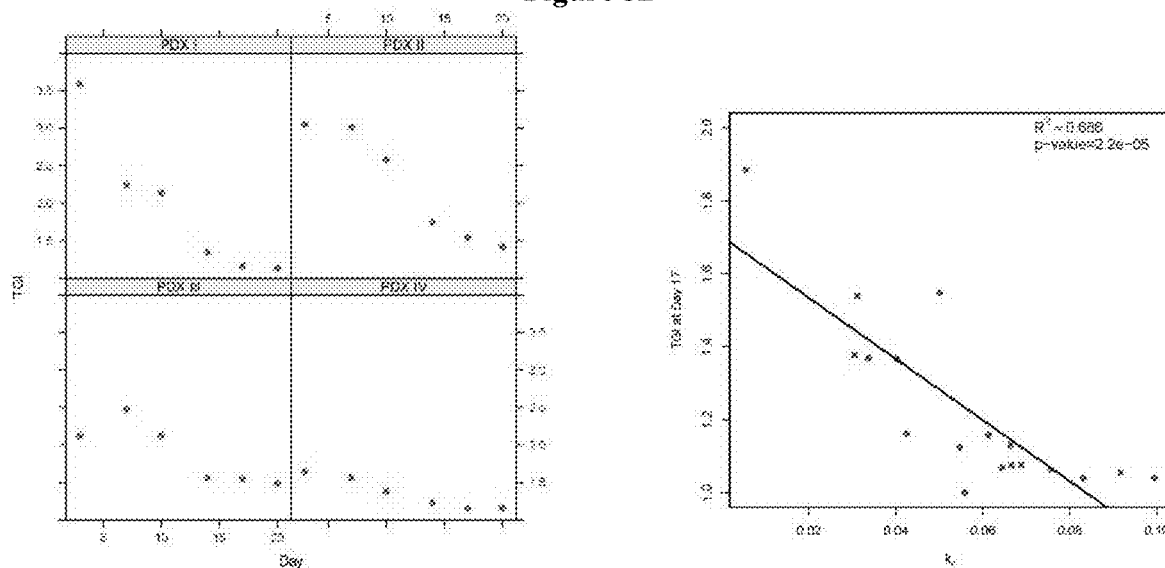
Figure 5E
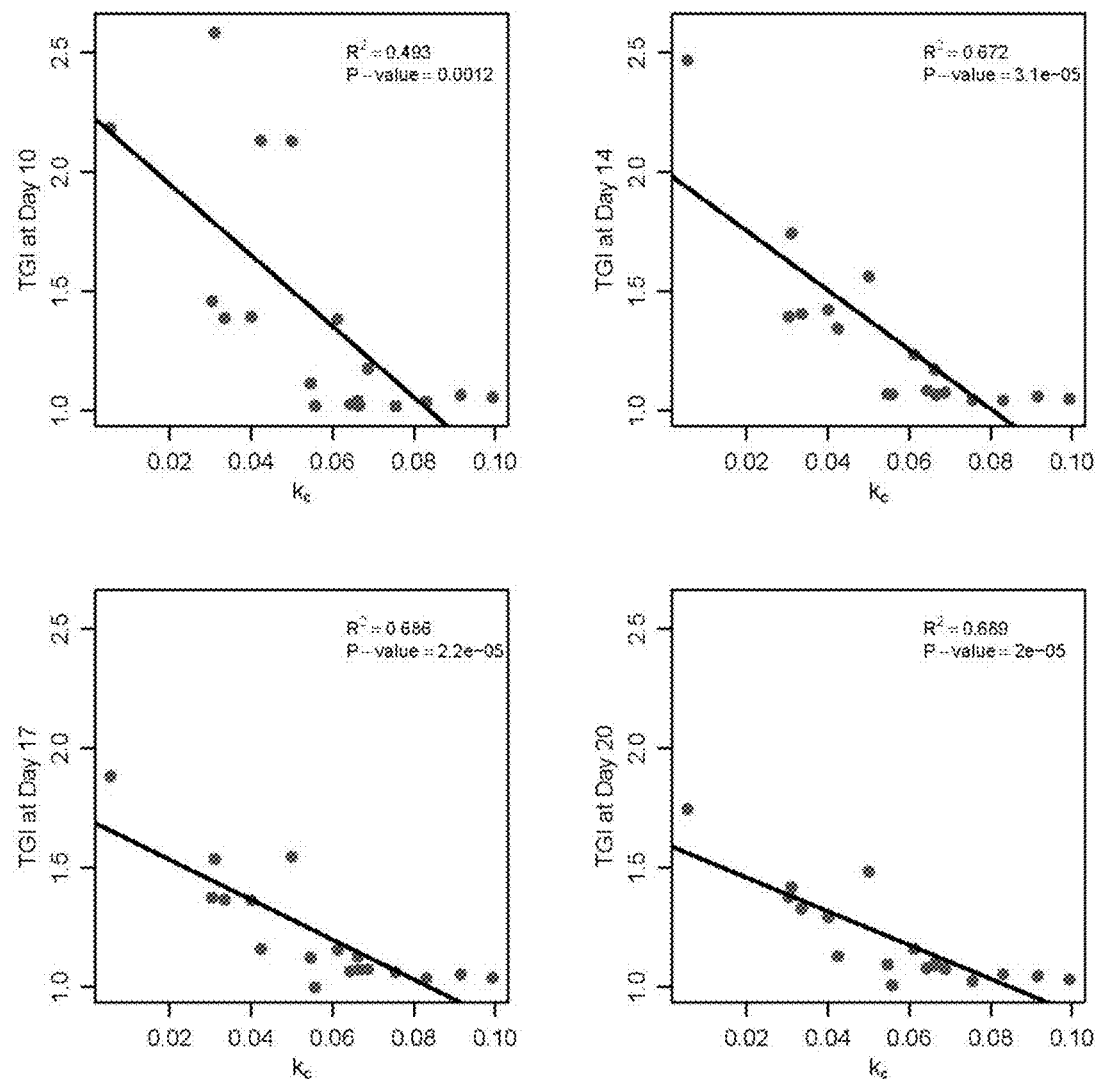
Figure 5F
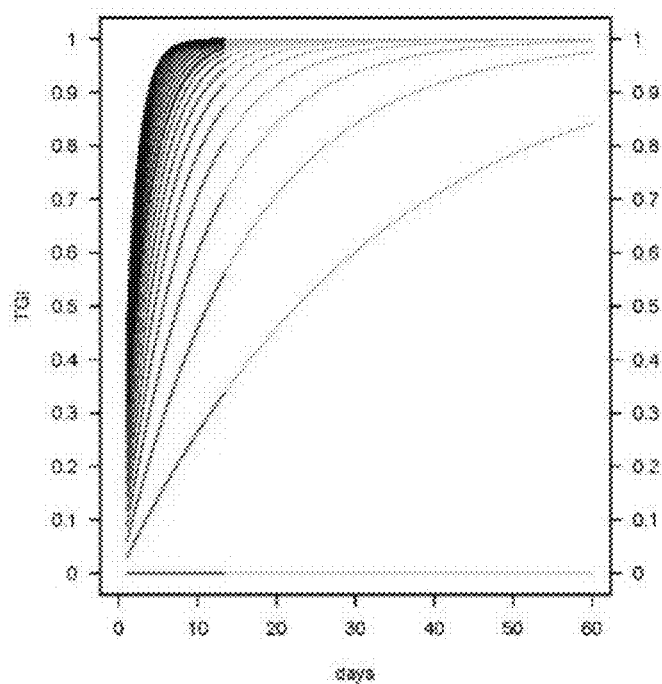
Figure 6A
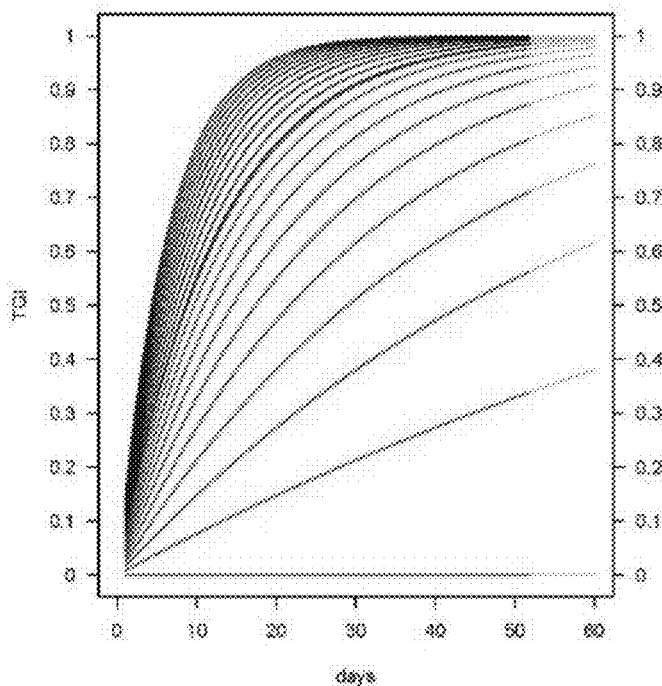
Figure 6B
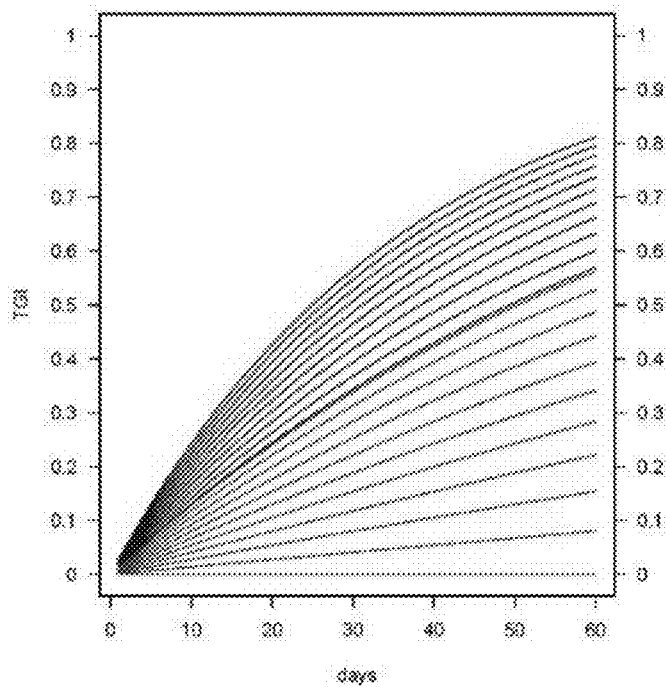
Figure 6C
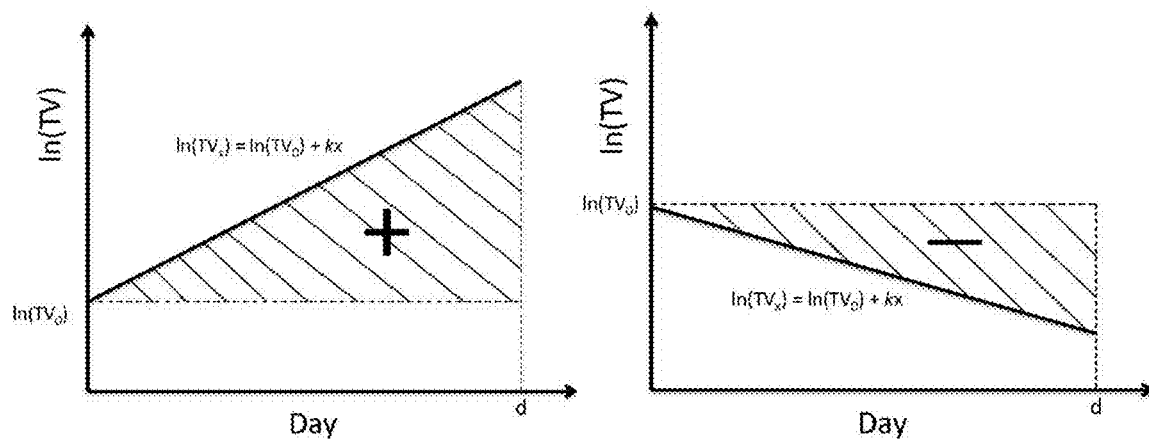
Figure 7A
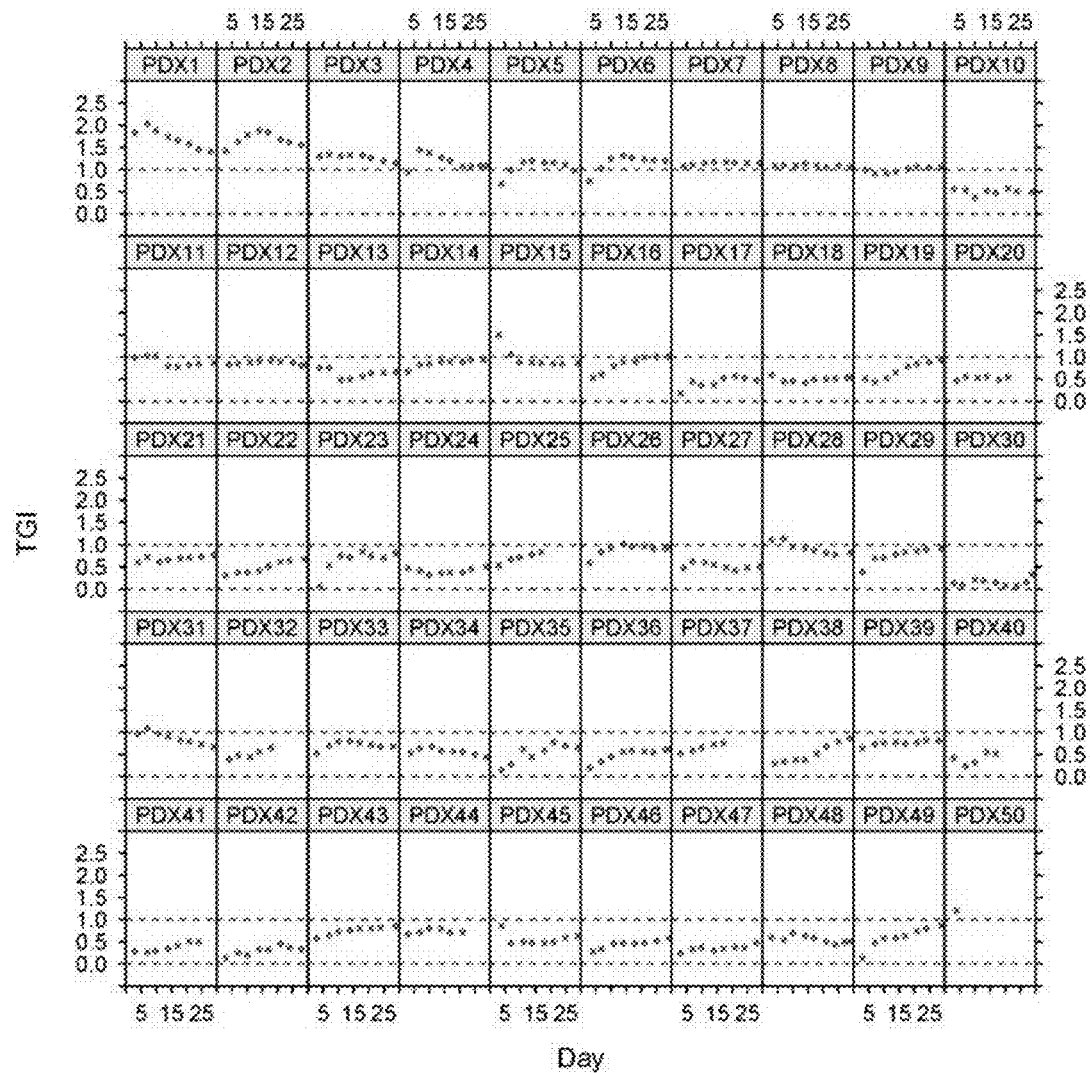
Figure 7B
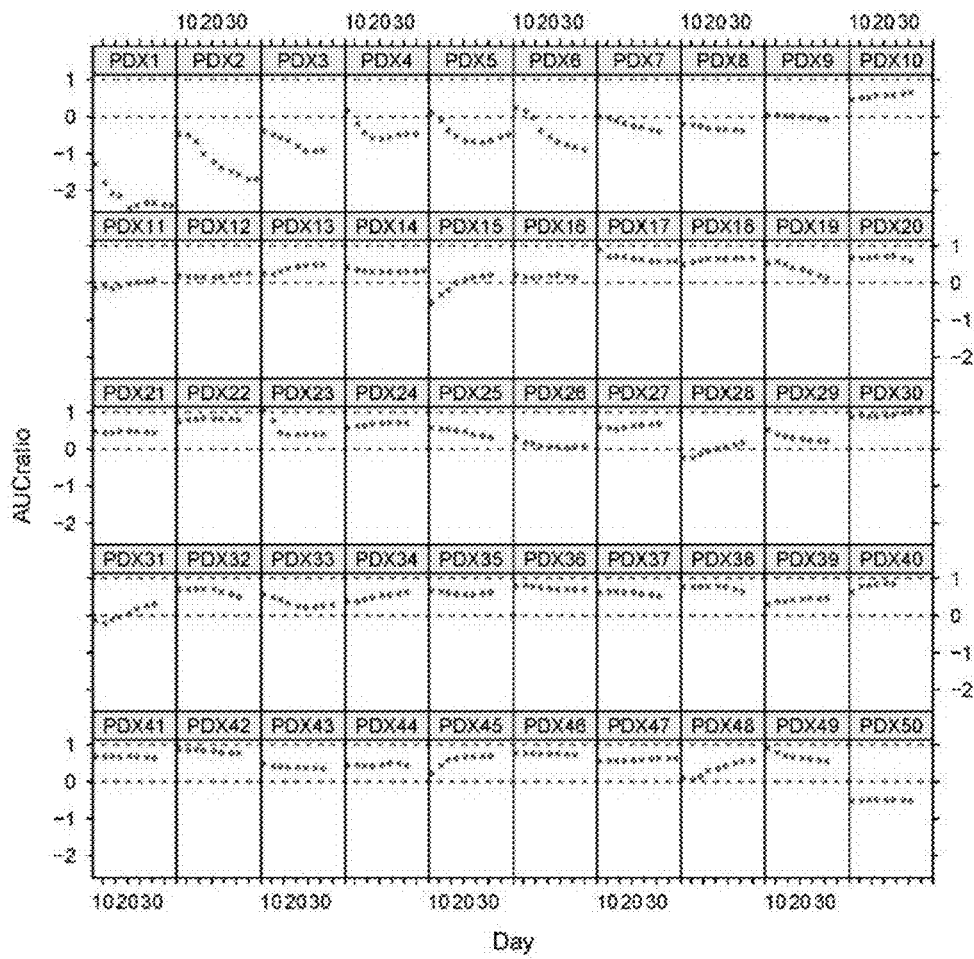
Figure 7C
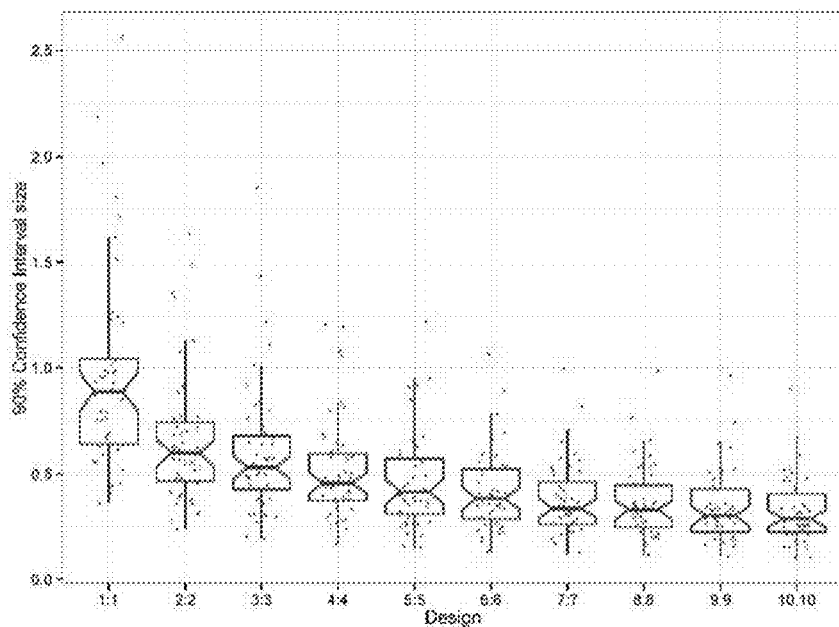
Figure 7D
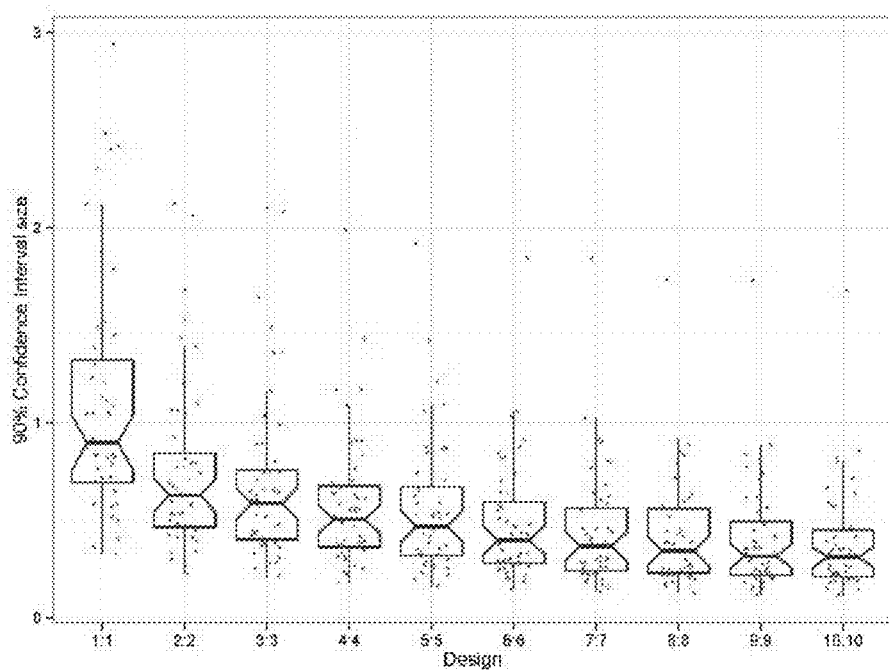
Figure 7E
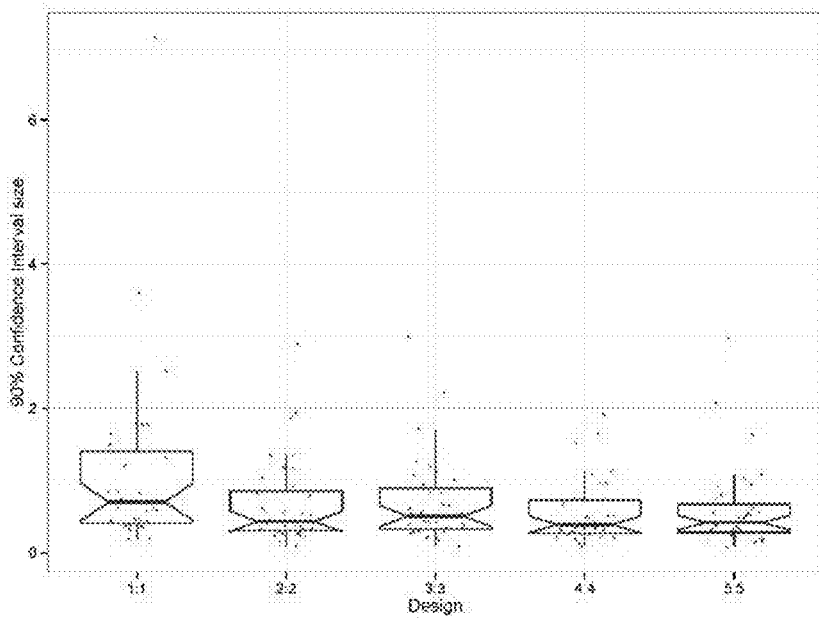
Figure 7F

Figure 7G

Figure 7H

$R^2 = 0.174$
p-value=0.03

TGI

EGFR expression (log_2FPKM)

Figure 8A

$R^2 = 0.455$
p-value=0.00011

AUC ratio

EGFR expression (log_2FPKM)
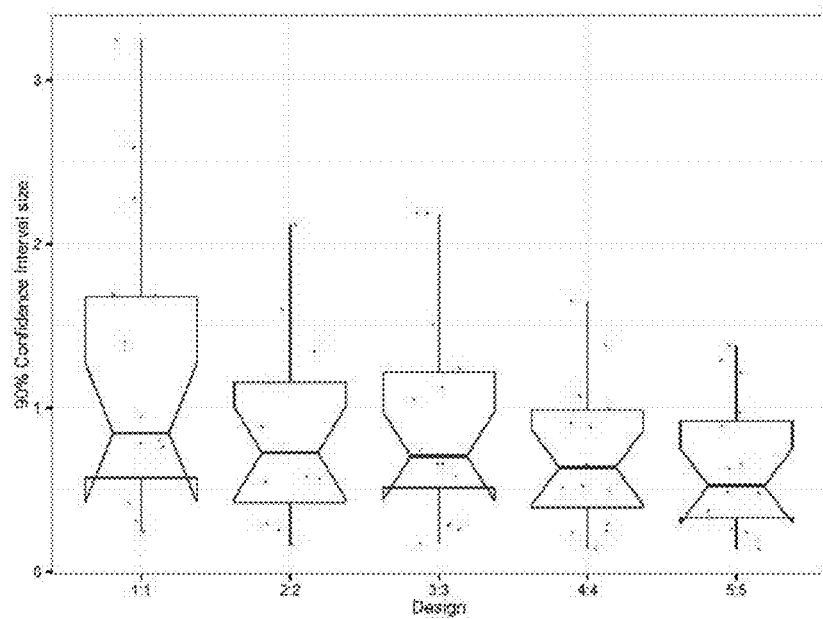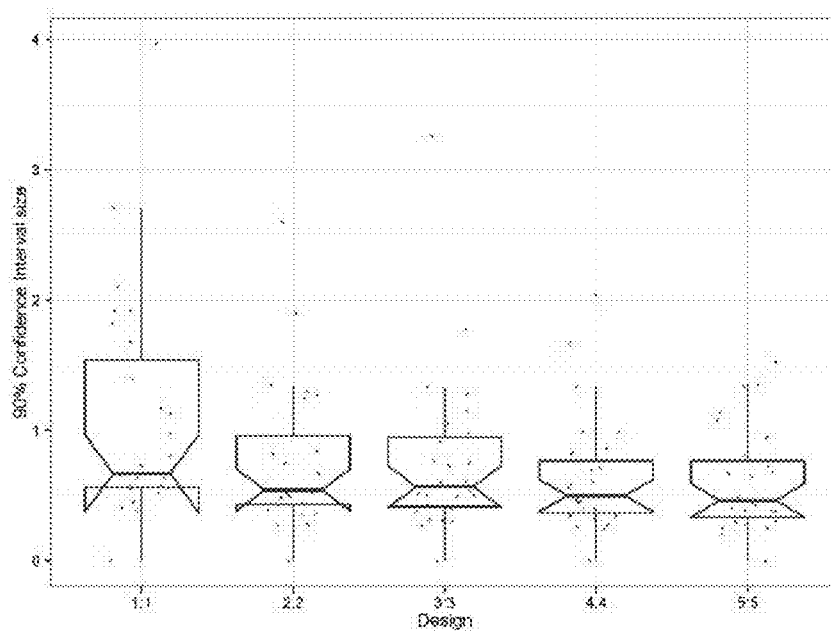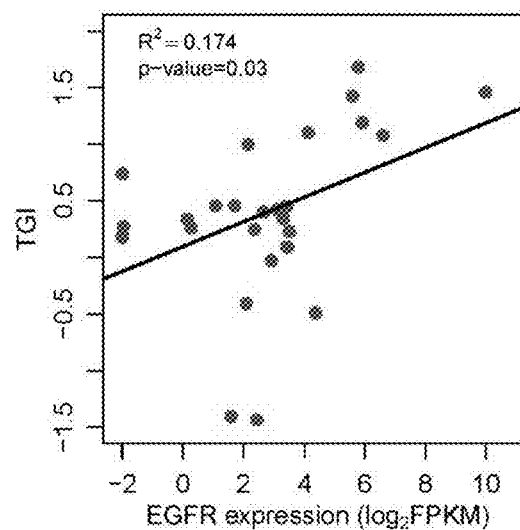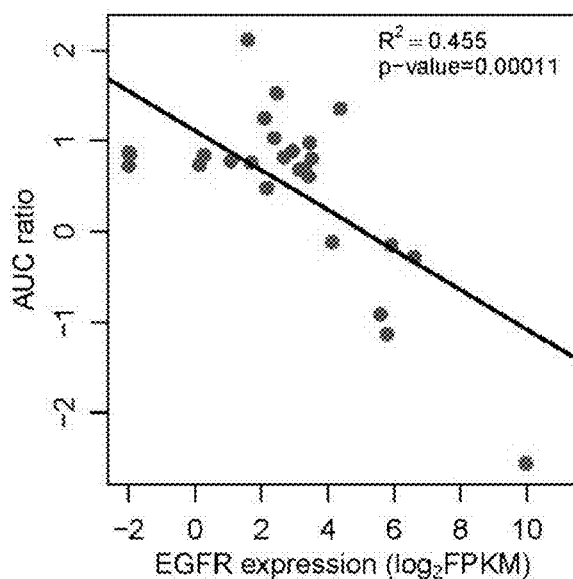
Figure 8B

Figure 9A

Vehicle
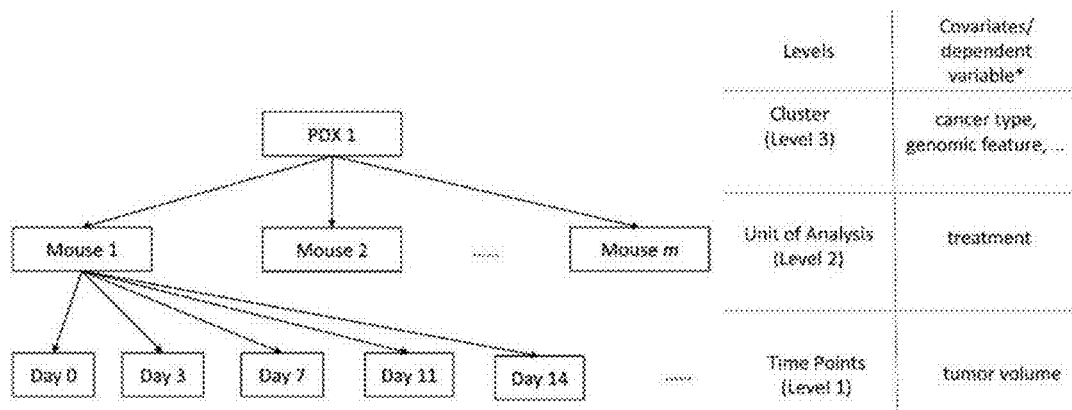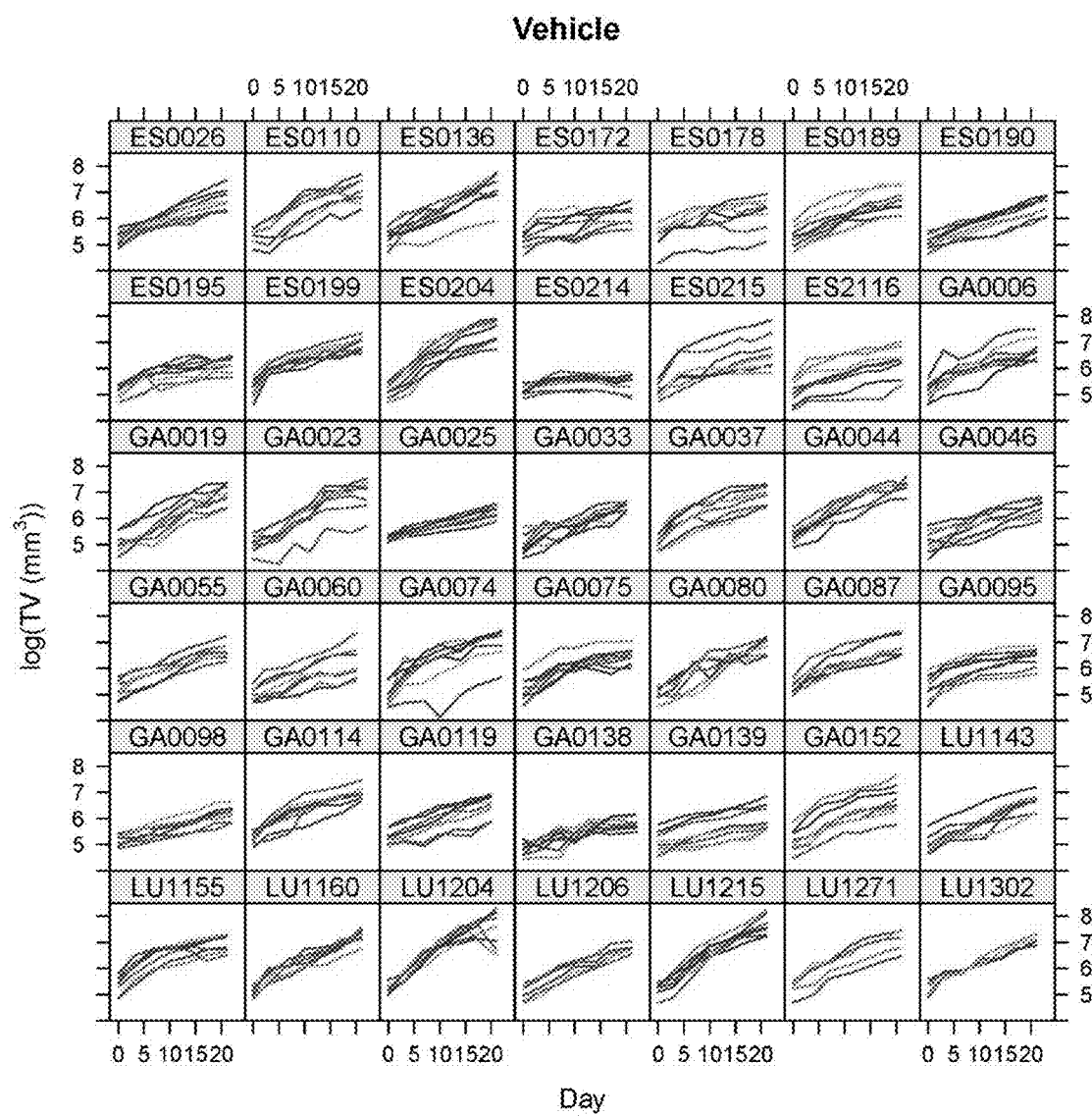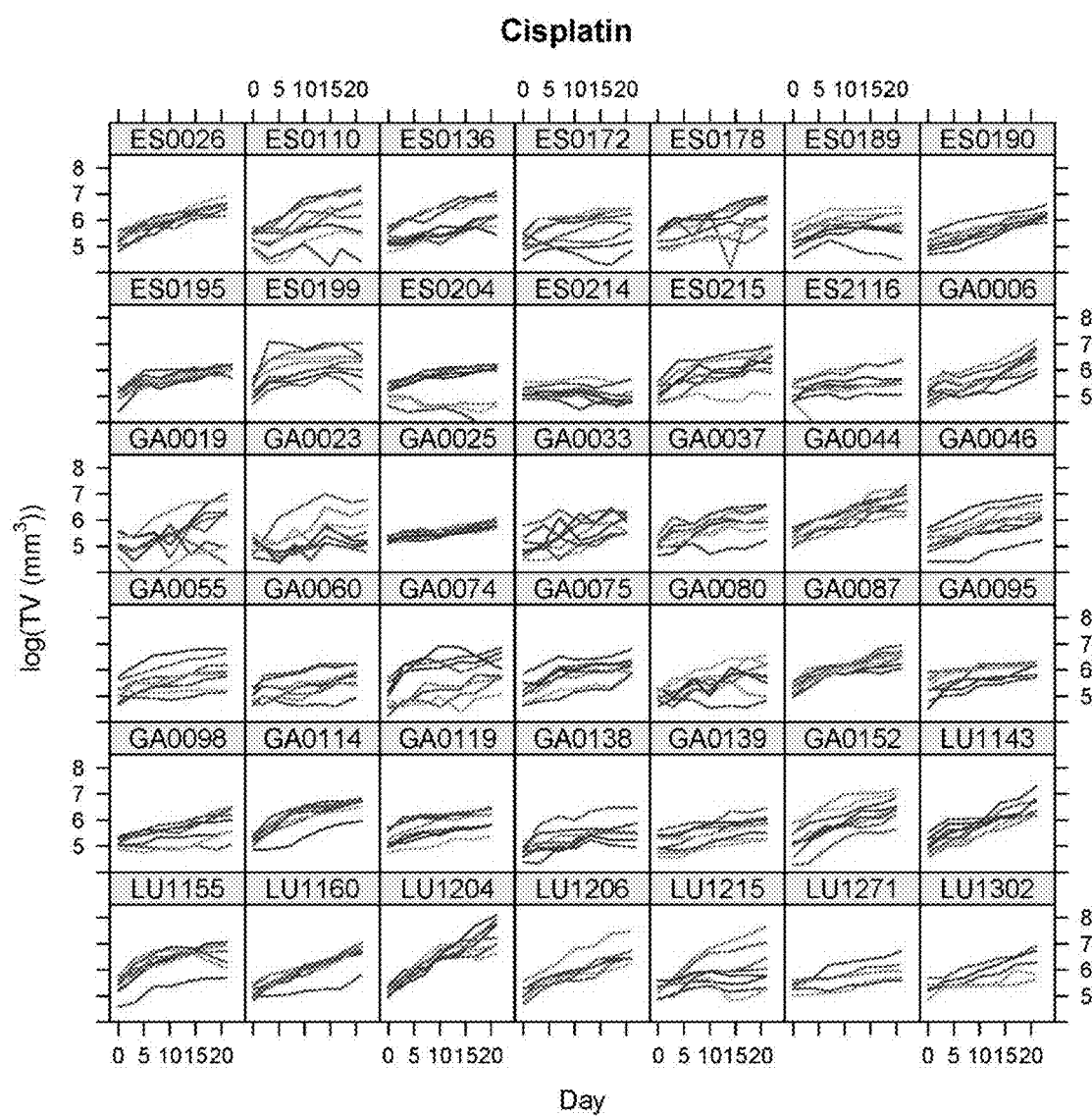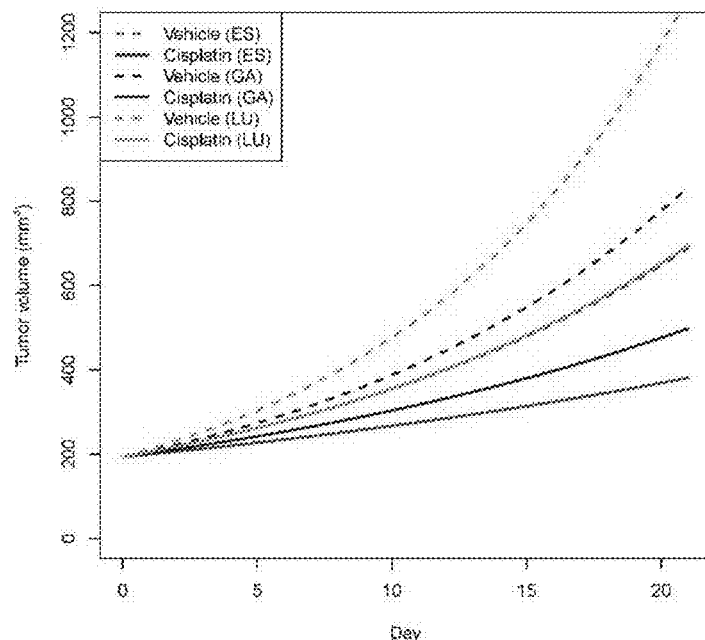
Figure 9B

Figure 9C

Figure 9D
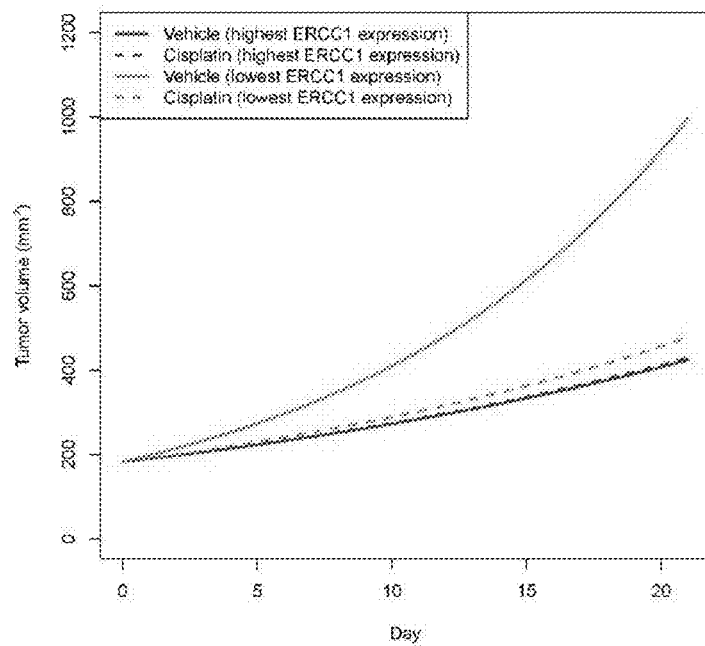
Figure 9E
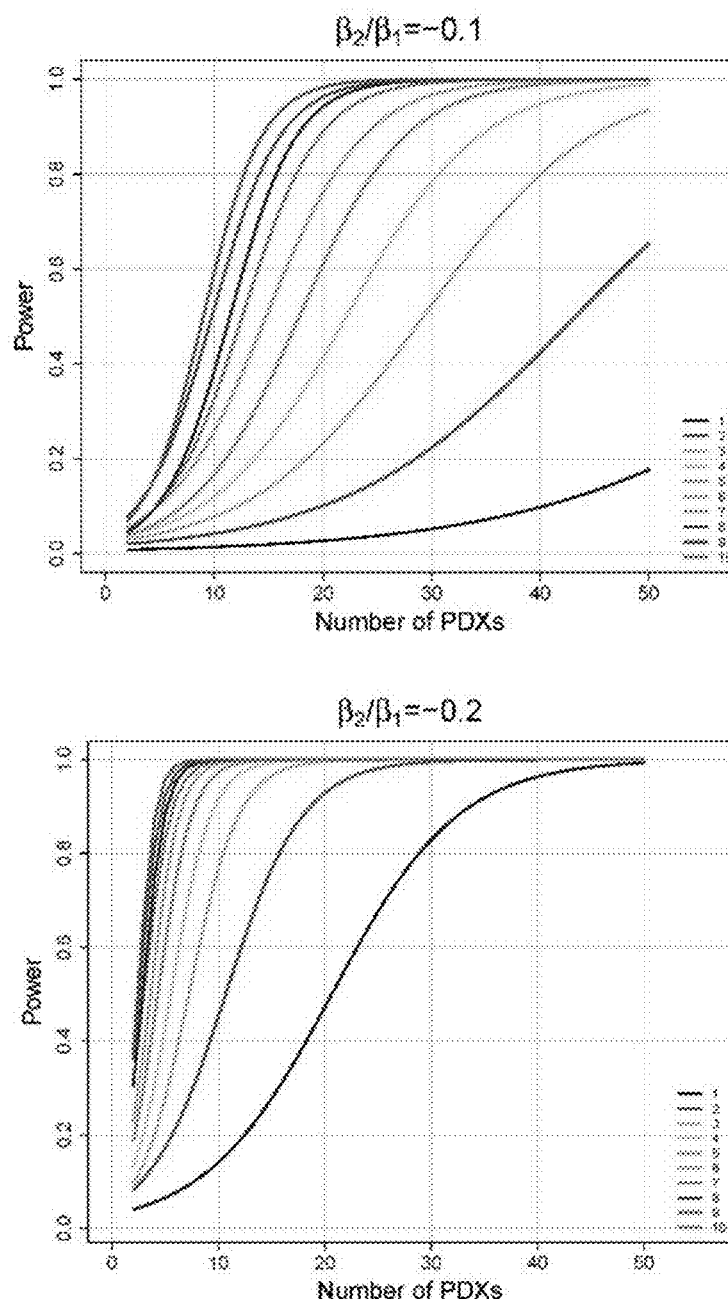
Figure 9F
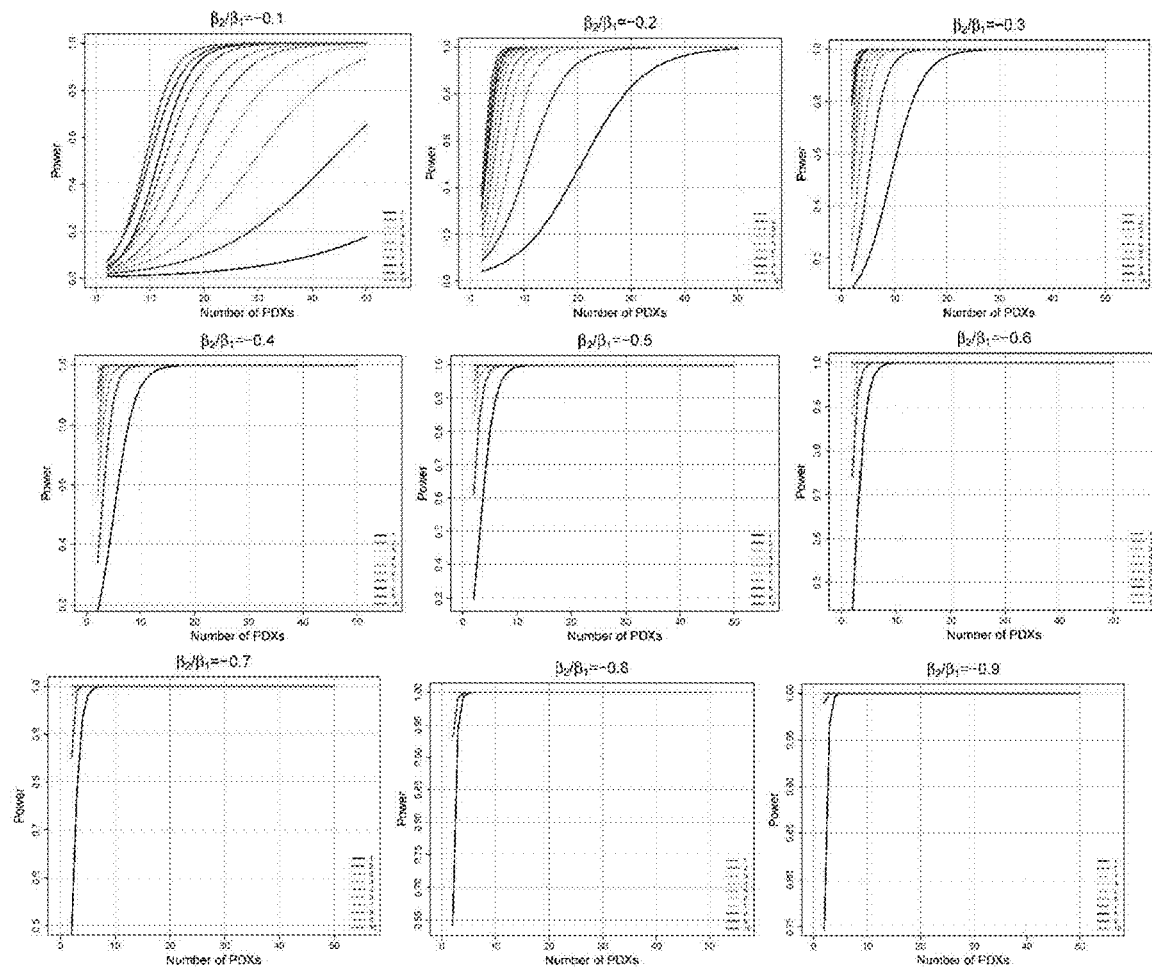
Figure 9G
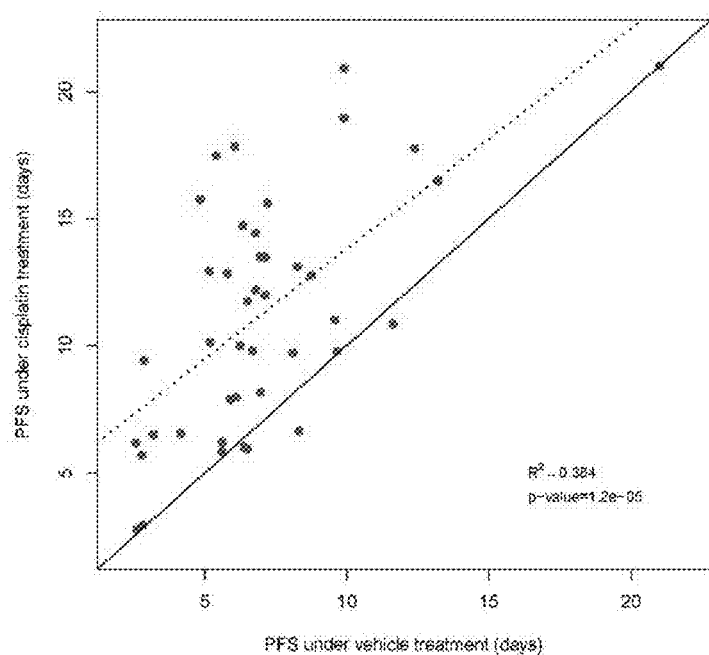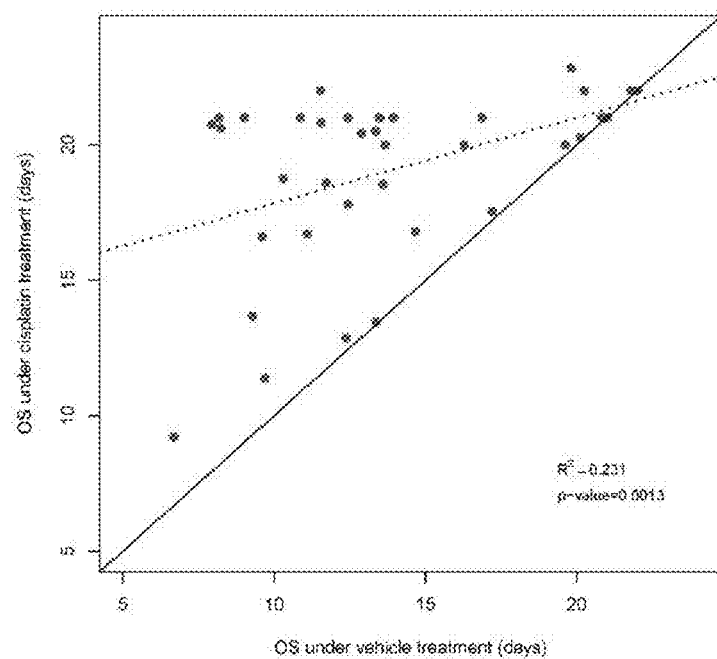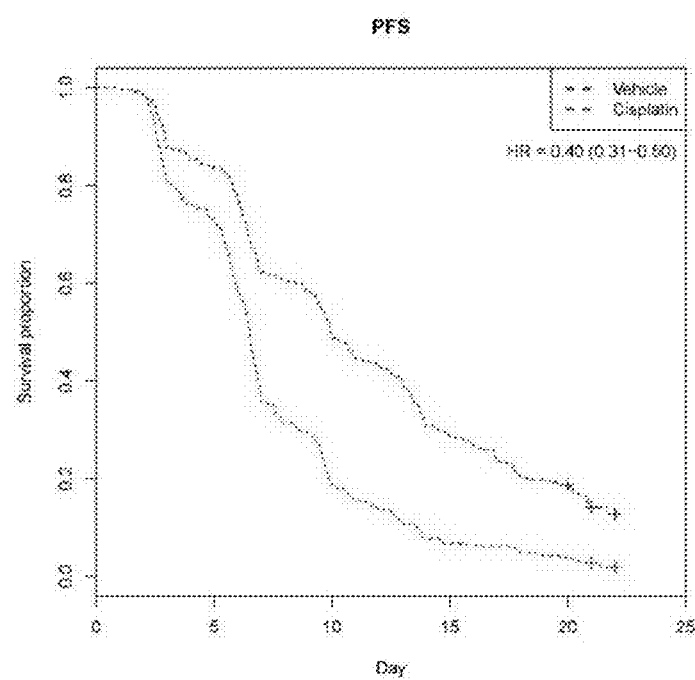
Figure 10A

Figure 10B

PFS
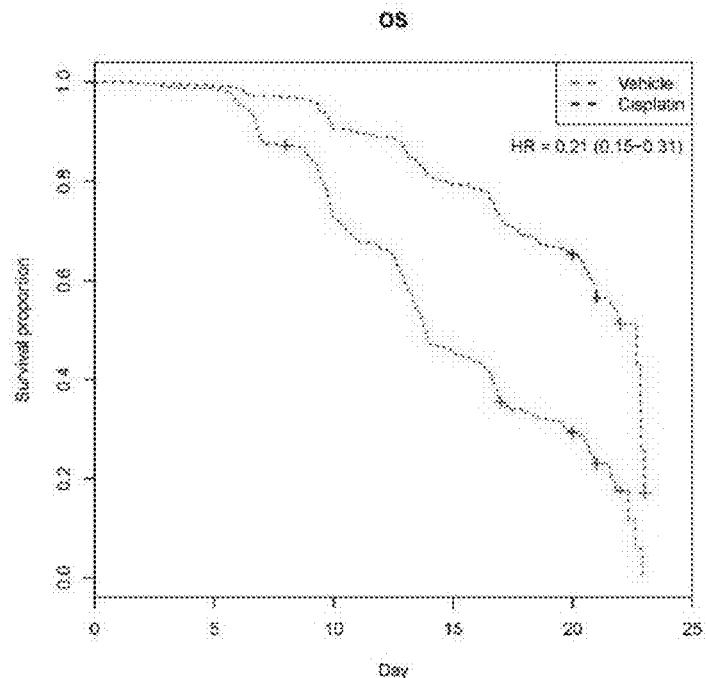
Figure 11A

Figure 11B
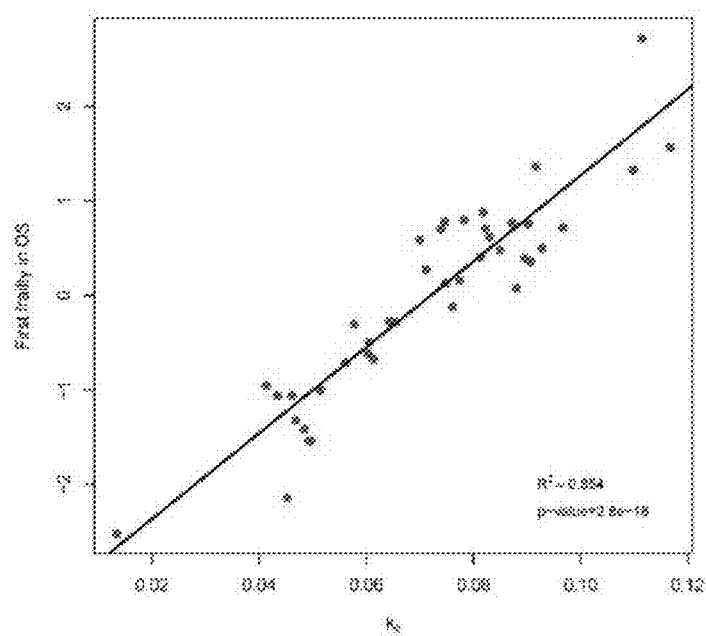
Figure 11C
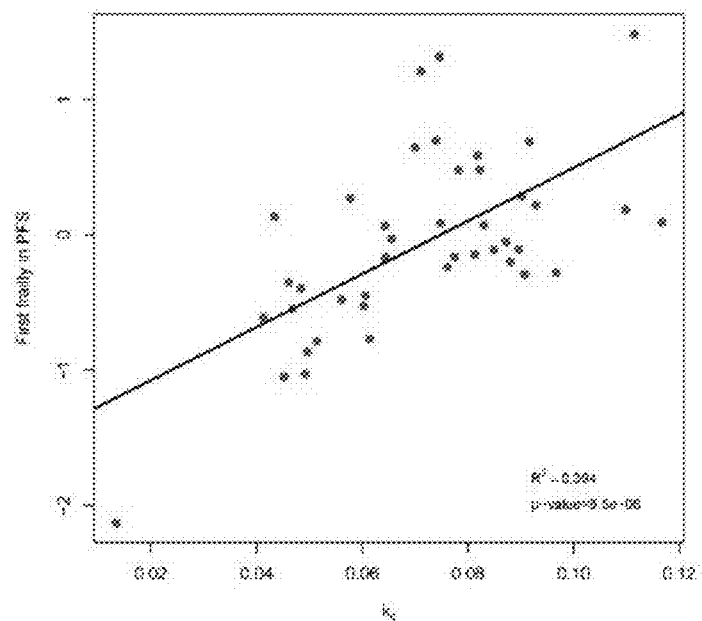
Figure 11D
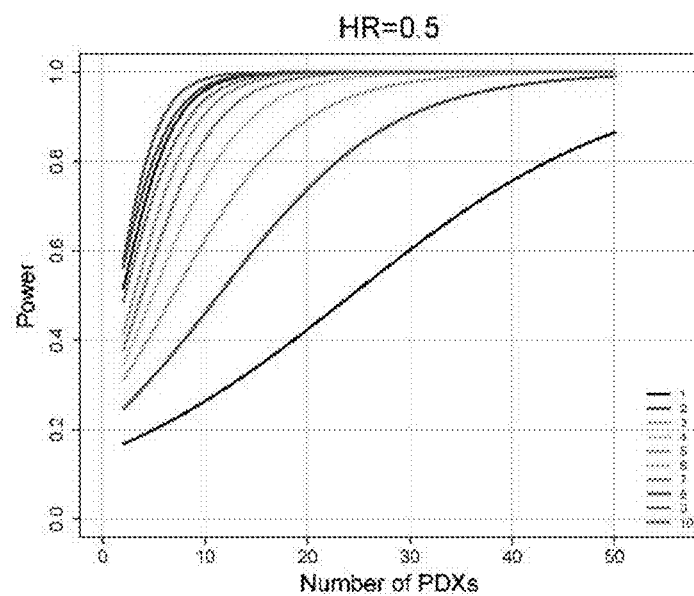
Figure 11E
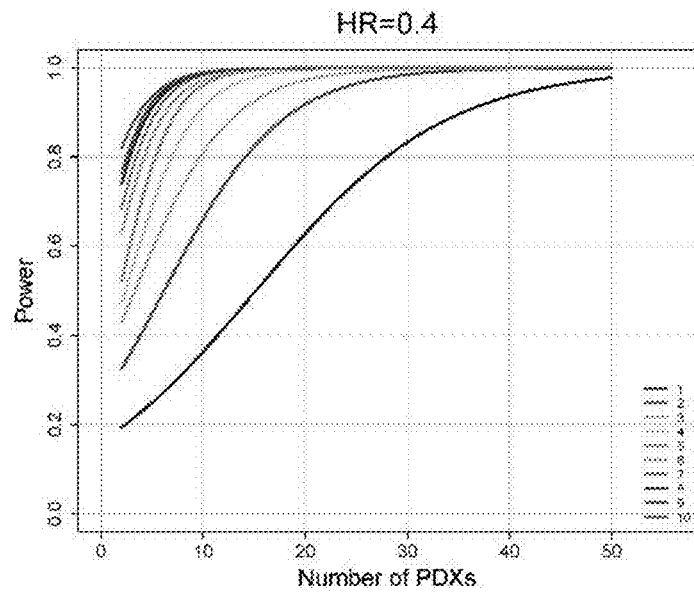
Figure 11F
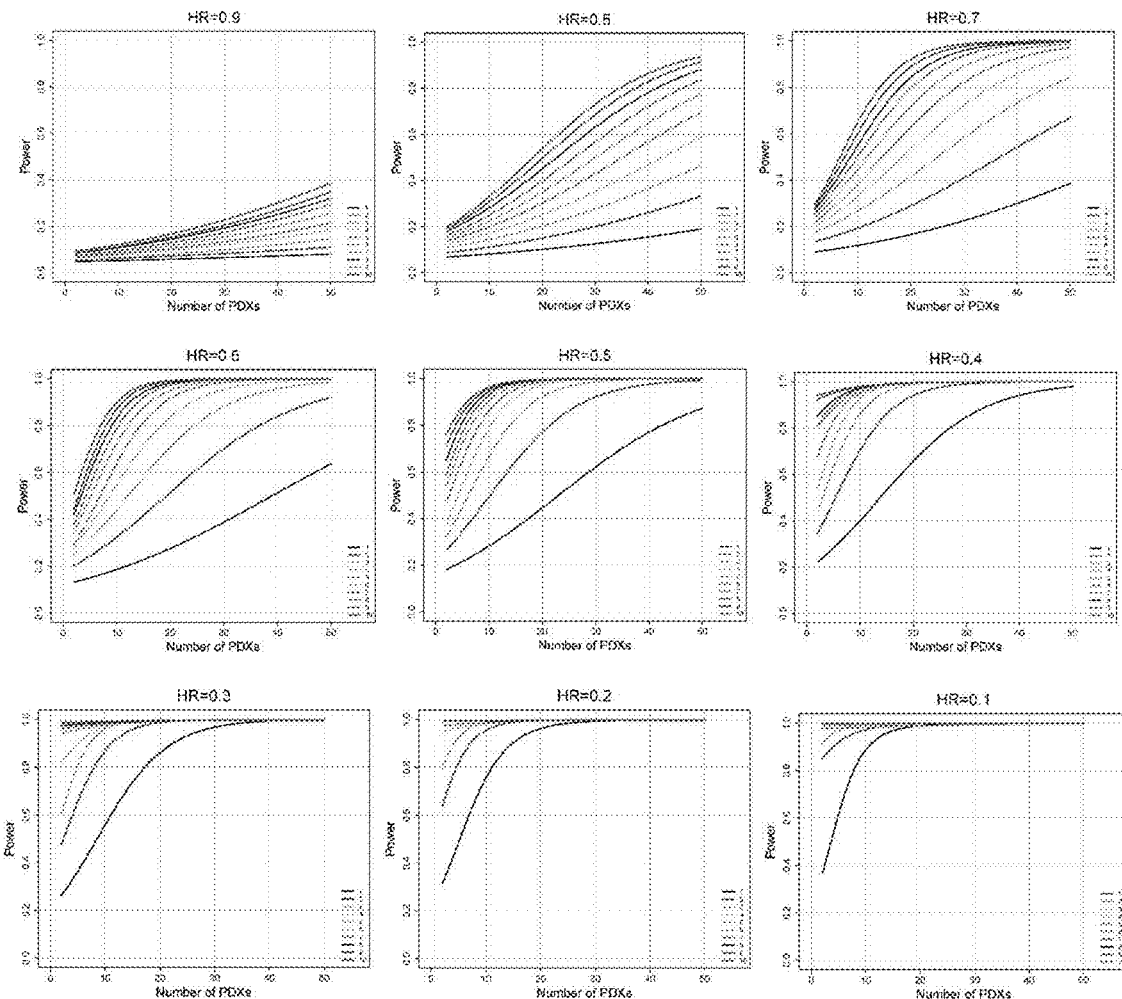
Figure 11G
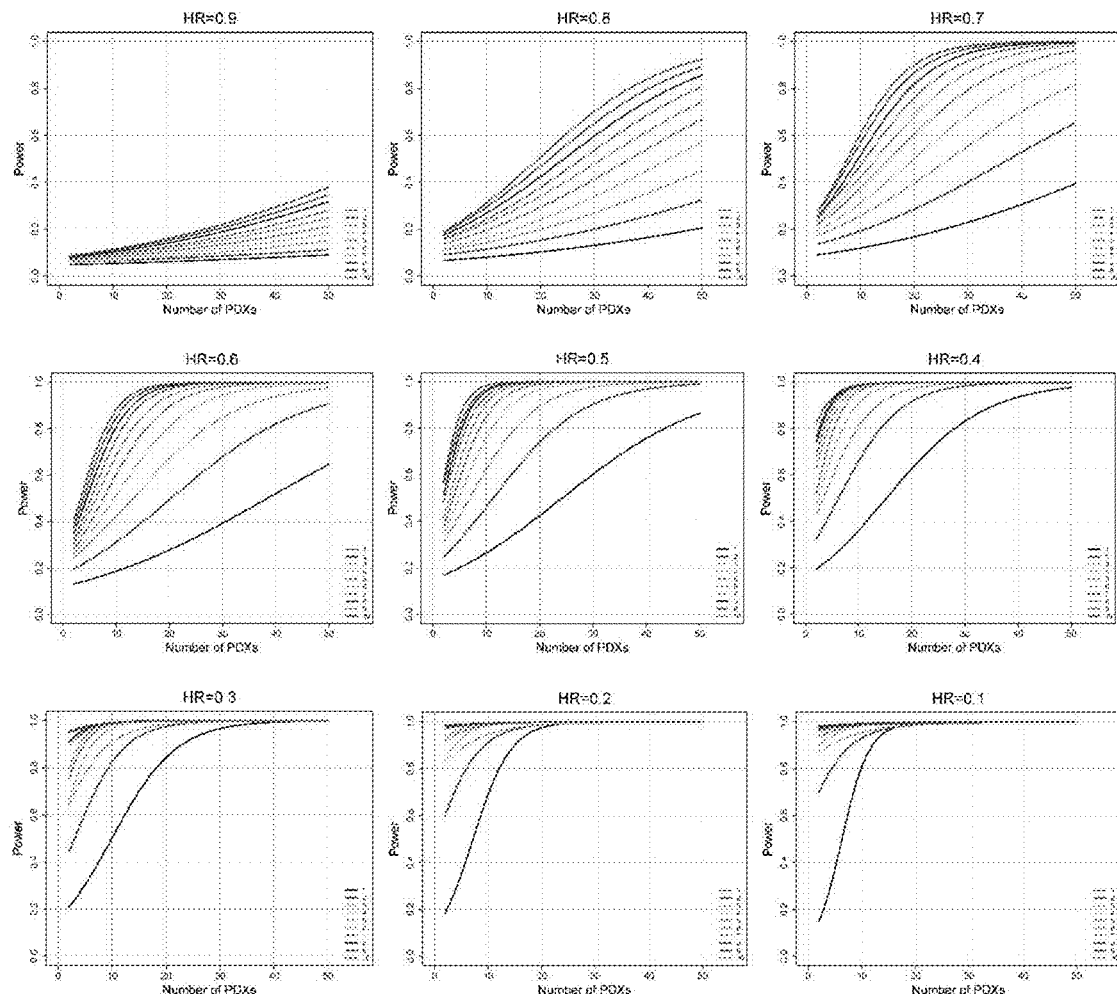
Figure 11H

METHODS OF MOUSE CLINICAL TRIAL

FIELD OF THE INVENTION

[0001] The present invention generally relates to conducting mouse clinical trials.

BACKGROUND OF THE INVENTION

[0002] Xenograft tumors, including patient-derived xenografts (PDXs), have been used as preclinical models for efficacy evaluation of cancer drugs (Povlsen C O and Rygaard J, Pathology (1971) 79(2):159-69; Castro J E, Nature: New biology (1972) 239(90):83-4; Cobb L M, British journal of cancer (1973) 28(5):400-11). With resemblance to patient tumors in histo-/molecular pathology, PDXs have faithful pharmacological response to treatment as seen in patients (Rosfjord E et al., Biochemical pharmacology (2014) 91(2):135-43; Hidalgo M et al., Cancer discovery (2014) 4(9):998-1013; Gao H et al., Nat Med (2015) 21(11):1318-25; Owonikoko T K et al., J Transl Med (2016) 14(1):111), more so than cell line-derived xenografts (Rosfjord E et al., Biochemical pharmacology (2014) 91(2): 135-43; Guo S et al., Cancer Res (2016); Tentler J J et al., Nat Rev Clin Oncol (2012) 9(6):338-50; DeRose Y S et al., Nat Med (2011) 17(11):1514-20; Zhang X et al., Cancer Res (2013) 73(15):4885-97; Zhao X et al., Neuro-oncology (2012) 14(5):574-83; Kabos P et al., Breast Cancer Res and Treatment (2012) 135(2):415-32). Availability of large collections of PDXs, representing diverse diseases (Julien S et al., Clinical Cancer Res (2012) 18(19):5314-28; Malaney P et al., Cancer Letters (2014) 344(1):1-12; Smith P G et al., Cancer Res (2014) 74(19 Supplement):1191-91; Budinska E and Popovici V, Mol Cancer Therapeutics (2014) 12(11_Supplement):A8-A8), supports population-based preclinical mouse clinical trials (MCTs) (Gao H et al., Nat Med (2015) 21(11):1318-25; Chen D et al., Oncotarget (2015) 6(38): 40815-21; Guo S et al., Oncotarget (2016); Guo S et al., Cancer Res (2016); Zhang L et al., Sci Rep (2013) 3:2992), mimicking human trials. Augmented with genomic annotations, such trial can be scientifically revealing. It would be all important and productive to have a comprehensive and scientific sound theory and methodology to guide and analyze these type of preclinical cancer pharmacology studies.

[0003] Tumor growth inhibition (TGI), as a primary tumor response endpoint in preclinical cancer pharmacology studies, may be inadequate due to its disparity with time and tumor growth rate, etc. Although other surrogate endpoints have been examined (Gao H et al., Nat Med (2015) 21(11): 1318-25; Teicher B A, Progress in Drug Res (2005) 63:43-66), there is still a need for identifying ones more objectively reflective of the true drug effect. In addition, the population-based MCT study faces additional issues in its design and data analysis, where inadequate scientific theory and practice may become obstacle to hinder its broadly application. Frequently encountered questions yet to be addressed include: what scientific questions can be asked in a given MCT, number of PDXs and mice in each arm are required to answer those questions, the need of control arm, optimal readouts for assessing test subjects' drug response and survival, the impact of drug potency on study design, and method to discover predictive biomarkers, etc. (Heitj an D F et al., Cancer Res (1993) 53(24):6042-50; Wu J et al., J Biopharmaceutical Statistics (2010) 20(5):954-64; Laajala T D et al., Clinical Cancer Res (2012) 18(16):4385-96; Zhao

L et al., Clinical Cancer Res (2011) 17(5):1057-64; Xia C et al., J Biometrics & Biostatistics (2013); Pierrillas P B et al., The AAPS J (2016); Choudhury K R et al., Statistics in Med (2010) 29(23):2399-409). Therefore, there is continuing needs develop new methodology for conducting mouse clinical trial.

BRIEF SUMMARY OF THE INVENTION

[0004] In one aspect, the present disclosure provides a method of conducting mouse clinical trial comprising the steps of:

[0005] receiving a dataset of tumor volumes measured in a mouse clinical trial, wherein the mouse clinical trial comprises the steps of:

[0006] obtaining a tumor sample derived from a patient;

[0007] grafting the tumor sample to a treatment group comprising m mice and a control group comprising n mice, wherein m and n are integers;

[0008] administering a drug to the treatment group;

[0009] administering a vehicle to the control group; and

[0010] measuring tumor volume of the treatment group and tumor volume of the control group at a plurality of days;

[0011] determining tumor growth curve of the treatment group and tumor growth curve of the control group;

[0012] determining area under curve (AUC) of the treatment group (AUC_T) and AUC of the control group (AUC_C); and

[0013] evaluating efficacy of the drug based on an AUC ratio between the AUC_T and the AUC_C.

[0014] In certain embodiments, $AUC_T = \int_0^{d(T)} \ln V_x^{(T)} dx - d(T) \times \ln V_0^{(T)}$, wherein $V_0^{(T)}$ is the tumor volume of the treatment group at day 0, $V_x^{(T)}$ is the tumor volume of the treatment group at day x, d(T) is the number of days the measuring step for the treatment group lasts; and

[0015] In certain embodiments, $AUC_C = \int_0^{d} \ln V_x^{(C)} dx - d \times \ln V_0^{(C)}$, wherein $V_0^{(C)}$ is the tumor volume of the control group at day 0, $V_x^{(C)}$ is the tumor volume of the control group at day x, d(C) is the number of days the measuring step for the treatment group lasts.

[0016] In certain embodiments, d(T)=d(C), wherein the

$$AUC \text{ ratio} = \frac{AUC_T}{AUC_C}.$$

[0017] In certain embodiments, d(T)≠d(C), wherein the

$$AUC \text{ ratio} = \frac{AUC_T/d(T)^2}{AUC_C/d(C)^2}.$$

[0018] In certain embodiments, m≥3 and n≥3. In certain embodiments, m=n.

[0019] In certain embodiments, the evaluating step comprises determining that the drug is effective when the AUC ratio is less than 1.

[0020] In certain embodiments, the method disclosed herein further comprises the step of determining correlation of a factor to the efficacy of the drug.

[0021] In certain embodiments, the factor is expression level of a gene. In one embodiment, the gene is EGFR and the drug is cetuximab.

[0022] In certain embodiments, the tumor volumes are between 100-300 mm^3.

[0023] In another aspect, the present disclosure provides a method of conducting mouse clinical trial comprising the steps of:

[0024] receiving a dataset of tumor volumes measured in a mouse clinical trial, wherein the mouse clinical trial comprises the steps of:

[0025] obtaining a tumor sample derived from a patient;

[0026] grafting the tumor sample to a treatment group comprising m mice and a control group comprising n mice, wherein m and n are integers;

[0027] administering a drug to the treatment group;

[0028] administering a vehicle to the control group; and

[0029] measuring tumor volume of the treatment group and tumor volume of the control group at a plurality of days;

[0030] evaluating impact of a factor on the tumor volume of the treatment group, wherein the tumor volume of the treatment group after logarithmic transformation has a linear relationship with the factor.

[0031] In certain embodiments, the factor is selected from the group consisting of: efficacy of the drug, cancer type of the patient, expression level of a gene, and existence of a mutation.

[0032] In one embodiment, the drug is cisplatin.

[0033] In certain embodiments, the cancer type is esophageal cancer, gastric cancer or lung cancer.

[0034] In once embodiments, the gene is ERCC.

[0035] In some embodiments, m≥3 and n≥3. In some embodiment, m=n.

[0036] In certain embodiments, the method disclosed herein further comprises conducting a second mouse clinical trial based on the impact of the factor determined in the evaluation step.

[0037] In yet another aspect, the present disclosure provides a method of conducting a mouse clinical trial, comprising

[0038] receiving a dataset of tumor volumes in a mouse clinical trial, wherein the mouse clinical trial comprises the steps of:

[0039] obtaining a plurality of tumor samples derived from a plurality of patients;

[0040] grafting the plurality of tumor samples to a treatment group of mice and a control group of mice;

[0041] administering a drug to the treatment group;

[0042] administering a vehicle to the control group; and

[0043] measuring tumor volume of the treatment group and tumor volume of the control group at a plurality of days;

[0044] determining progress-free survival (PFS) or overall survival (OS) of the treatment group and the control group;

[0045] evaluating efficacy of the drug based on the PFS or OS using an additive frailty model.

[0046] In certain embodiments, the additive frailty model includes a hazard function, wherein the hazard function for the j-th mouse of the i-th PDX is

$$h_{ij}(t) = h_0(t)\exp(u_i + (w + v_i)T_{ij} + \beta^T X_i)$$

wherein h_0 (t) is a baseline hazard function, u_i is a random effect associated with the i-th patient without drug treatment, w is mean drug effect, v_i is a random effect associated the i-th patient that depicts drug response deviating from w, T_{ij} is 0 for the control group and 1 for the treatment group, X_i is a vector for a covariate of the plurality of patients, β^T is a vector quantifying fixed effects of the covariate.

[0047] In certain embodiments, the PFS is the time until the tumor volume doubles.

[0048] In certain embodiments, the covariate is cancer type, expression of a gene or a gene mutation.

[0049] In certain embodiments, the treatment group consists of n mice for each patient and the control group consists of n mice for each patient, wherein n≥3.

[0050] In certain embodiments, the method disclosed herein further comprises conducting a second mouse clinical trial based on the hazard function.

BRIEF DESCRIPTION OF THE FIGURES

[0051] FIG. 1 illustrates tumor volume doubling time (DT) in PDXs for 10 cancers ranked by increasing median DT. LI: liver, BR: breast, PA: pancreatic, OV: ovarian, CR: colorectal, LU: lung, ES: esophageal, GL: gallbladder, GA: gastric, HN: head and neck.

[0052] FIG. 2 illustrates that in drug groups, the coefficient of determination (R^2) by Equation 2 is smallest when the TV ratio between end and start days is around 1. When the TV ratio is larger than 2 and 3, there are 91.8% and 95.1% growth curves with R^2>0.70.

[0053] FIG. 3A illustrates the relative distance of growth curves under drug treatment and vehicle treatment, visualized by the first two t-SNE dimensions (van der Maatern & Hintton, J machine Learning Res (2008) 2579-2605). A total of 300 randomly selected growth curves were used including 250 under drug treatment and 50 under vehicle treatment, close to the ratio in the total set of 34081 growth curves. For each growth curve, its 480×480 jpeg file was converted into a numeric matrix of the same dimension and used as input to the R Rtsne package (Krijthe J CRAN (2015)). About 20% of growth curves under drug treatment form a separated cluster in the upper part of the graph.

[0054] FIG. 3B illustrates the visualization of all 34081 growth curves. The isolated cluster includes irregular growth curves that are not linear, or have V-like or A-like shapes.

[0055] FIG. 4A illustrates the variation of TGI by day and by drug efficacy in PDXs with fastest growth rate, i.e. k_C, based on Equation 4 with $k_T \leq k_C$. The red lines are TGIs for k_T/k_C ranging from 0 to 1 with 0.1 stepwise increase from bottom to top; the blue lines are TGIs for k_T/k_C ranging from 2 to 1 with 0.1 stepwise decrease from top to bottom. Both red and blue lines are drawn with slight separation for TGI=1. Gray portion of the lines means that the tumor volumes are larger than 3000 mm^3, at which mice are sacrificed and TGIs no longer exist.

[0056] FIG. 4B illustrates the variation of TGI by day and by drug efficacy in PDXs with median growth rate, i.e. k_C, based on Equation 4 with $k_T \leq k_C$. The red lines are TGIs for k_T/k_C ranging from 0 to 1 with 0.1 stepwise increase from bottom to top; the blue lines are TGIs for k_T/k_C ranging from 2 to 1 with 0.1 stepwise decrease from top to bottom. Both red and blue lines are drawn with slight separation for

3

TGI=1. Gray portion of the lines means that the tumor volumes are larger than 3000 mm^3, at which mice are sacrificed and TGIs no longer exist.

[0057] FIG. **4C** illustrates the variation of TGI by day and by drug efficacy in PDXs with slowest growth rate, i.e. k_C, based on Equation 4 with $k_T \leq k_C$. The red lines are TGIs for k_T/k_C ranging from 0 to 1 with 0.1 stepwise increase from bottom to top; the blue lines are TGIs for k_T/k_C ranging from 2 to 1 with 0.1 stepwise decrease from top to bottom. Both red and blue lines are drawn with slight separation for TGI=1. Gray portion of the lines means that the tumor volumes are larger than 3000 mm^3, at which mice are sacrificed and TGIs no longer exist.

[0058] FIG. **5A** illustrates TGI at day 3, 7, 10, 14, 17, and 21 for 40 PDXs in a MCT. The average starting tumor volumes are between 115 mm^3~194 mm^3, and differ by 4.7% on average between the drug and vehicle groups for a PDX. TGI is calculated by Equation 3.

[0059] FIG. **5B** illustrates TGIs at 6 measurement days for the first 4 PDXs in a MCT as shown in FIG. **5A**. TGI increases by day when it is between 0 and 1. A strong positive correlation is observed between tumor growth rate k_c and TGI at day 17 for 24 PDXs whose TGIs are between 0 and 1 for all measurement days.

[0060] FIG. **5C** illustrates when between 0 and 100%, TGI is positive correlated with vehicle tumor growth rate k_c. The graphs show a set of 24 PDXs with TGIs less than 100% at all 4 measurement days from FIG. **5A**.

[0061] FIG. **5D** illustrates TGI at day 3, 7, 10, 14, 17, and 20 for 38 PDXs in a second MCT. TGI is calculated by Equation 3.

[0062] FIG. **5E** illustrates TGIs at 6 measurement days for the first 4 PDXs in the second MCT as illustrated in FIG. **5D**. TGI decreases by day when it is greater than 1. A strong negative correlation is observed between tumor growth rate k_c and TGI at day 17 for 18 PDXs whose TGIs are greater than 1 at all measurement days.

[0063] FIG. **5F** illustrates when greater than 100%, TGI is negatively correlated with vehicle tumor growth rate k_c. The graphs show a set of 18 PDXs with TGI greater than 100% at all 4 measurement days from FIG. **5D**.

[0064] FIG. **6A** illustrates TGI is a growth rate biased and time-dependent efficacy metric. The variation of TGI by day and by drug efficacy in PDXs with fastest growth rate, i.e. k_C, based on Equation

$$TGI = 1 - \frac{e^{k^T x}}{e^{k^C x}}$$

with $k_T \leq k_C$. The red lines are TGIs for k_T/k_C ranging from 0 to 1 with 0.1 stepwise increase from bottom to top, the blue lines are TGIs for k_T/k_C ranging from 2 to 1 with 0.1 stepwise decrease from top to bottom. Both red and blue lines are drawn with slight separation for $k_T = k_C$. Gray portion of the lines means that the tumor volumes are larger than 3000 mm^3, at which mice are sacrificed and TGIs no longer exist.

$$TGI = 1 - \frac{e^{k^T x}}{e^{k^C x}}$$

with $k_T \leq k_C$. The red lines are TGIs for k_T/k_C ranging from 0 to 1 with 0.1 stepwise increase from bottom to top, the blue lines are TGIs for k_T/k_C ranging from 2 to 1 with 0.1 stepwise decrease from top to bottom. Both red and blue lines are drawn with slight separation for $k_T = k_C$. Gray portion of the lines means that the tumor volumes are larger than 3000 mm^3, at which mice are sacrificed and TGIs no longer exist.

[0066] FIG. **6C** illustrates TGI is a growth rate biased and time-dependent efficacy metric. The variation of TGI by day and by drug efficacy in PDXs with slowest growth rate, i.e. k_C, based on Equation

$$TGI = 1 - \frac{e^{k^T x}}{e^{k^C x}}$$

with $k_T \leq k_C$. The red lines are TGIs for k_T/k_C ranging from 0 to 1 with 0.1 stepwise increase from bottom to top, the blue lines are TGIs for k_T/k_C ranging from 2 to 1 with 0.1 stepwise decrease from top to bottom. Both red and blue lines are drawn with slight separation for $k_T = k_C$. Gray portion of the lines means that the tumor volumes are larger than 3000 mm^3, at which mice are sacrificed and TGIs no longer exist.

[0067] FIG. **7A** is chematic illustrations of AUC. AUC is positive when tumor grows, and is negative when tumor shrinks.

[0068] FIG. **7B** illustrates efficacy end points of TGI for 50 PDXs in a MCT, each PDX has 10 mice each in the vehicle group and the drug group.

[0069] FIG. **7C** illustrates efficacy end points of AUC for 50 PDXs in the MCT as shown in FIG. **7B**, each PDX has 10 mice each in the vehicle group and the drug group.

[0070] FIG. **7D** illustrates the bootstrap 90% confidence interval sizes of AUC ratios under n:n design, based on efficacy data for 50 PDXs in the MCT as shown in FIGS. **7B** and **7C** with 10 mice each in the vehicle group and the drug group.

[0071] FIG. **7E** illustrates the bootstrap 90% confidence interval sizes for AUC ratios in a MCT of one embodiment. The n:n design means there are n mice in both the vehicle group and the drug group.

[0072] FIG. **7F** illustrates the bootstrap 90% confidence interval sizes for AUC ratios in a MCT of one embodiment. The n:n design means there are n mice in both the vehicle group and the drug group.

[0073] FIG. **7G** illustrates the bootstrap 90% confidence interval sizes for AUC ratios in a MCT of one embodiment. The n:n design means there are n mice in both the vehicle group and the drug group.

[0074] FIG. **7H** illustrates the bootstrap 90% confidence interval sizes for AUC ratios in a MCT of one embodiment. The n:n design means there are n mice in both the vehicle group and the drug group.

[0075] FIG. **8A** illustrates the correlation between EGFR expression and efficacy end points of TGI in a set of 27 gastric cancer PDXs treated with cetuximab.

[0076] FIG. **8**B illustrates the correlation between EGFR expression and efficacy end points of AUC ratio in the set of 27 gastric cancer PDXs treated with cetuximab as shown in FIG. **8**A.

[0077] FIG. **9**A illustrates the structure of the clustered longitudinal data for a PDX in a MCT. PDX level and mouse level covariates can be incorporated into the models.

[0078] FIG. **9**B illustrates the growth curve of 42 PDXs under vehicle treatment.

[0079] FIG. **9**C illustrates the growth curve of 42 PDXs under cisplatin treatment. Each mouse received cisplatin at 4 mg/kg, daily for 3 weeks.

[0080] FIG. **9**D illustrates the fitted tumor growth curves for 3 cancers under vehicle treatment and drug treatment by Equation 7.

[0081] FIG. **9**E illustrates the fitted growth curves for gastric cancer PDXs with highest and lowest ERCC1 mRNA expression by Equation 8.

[0082] FIG. **9**F illustrates the power curves at significance level $\alpha=0.05$ when treatment reduces tumor growth rate by 10% and 20%, i.e. $\beta_1/\beta_2=-0.1$ and -0.2 in Equation 9. The 10 colored curves in each graph denote the number of mice for every PDX.

[0083] FIG. **9**G illustrates the power curves at significance level $\alpha=0.05$ when treatment reduces tumor growth rate by 10% to 90%, i.e. $\beta_1/\beta_2=-0.1$ to -0.9 in Equation 9. The 10 colored curves in each graph denote the number of mice for every PDX.

[0084] FIG. **10**A illustrates that the median PFS values for PDXs under vehicle treatment and cisplatin treatment are highly correlated. The graphs use data from the cisplatin dataset as shown in FIGS. **9**B-**9**C.

[0085] FIG. **10**B illustrates that the median OS values for PDXs under vehicle treatment and cisplatin treatment are highly correlated. The graphs use data from the cisplatin dataset as shown in FIGS. **9**B-**9**C.

[0086] FIG. **11**A illustrates the survival curves under vehicle and drug treatments for PFS end points.

[0087] FIG. **11**B illustrates the survival curves under vehicle and drug treatments for OS end points.

[0088] FIG. **11**C illustrates the first frailty term u_i in Equation 10 is positively correlated with the tumor growth rate k_c in OS survival analysis.

[0089] FIG. **11**D illustrates the first frailty term u_i in Equation 10 is positively correlated with the tumor growth rate k_c in PFS survival analysis.

[0090] FIG. **11**E illustrates the power curves at significance level $\alpha=0.05$ when the hazard ratio is 0.5 for OS survival analysis. The 10 colored curves in each graph denote the number of mice for every PDX.

[0091] FIG. **11**F illustrates the power curves at significance level $\alpha=0.05$ when the hazard ratio is 0.4 for OS survival analysis. The 10 colored curves in each graph denote the number of mice for every PDX.

[0092] FIG. **11**G illustrates the power curves at significance level $\alpha=0.05$ when the hazard ratio is between 0.1 and 0. 9 in PFS analysis for the cisplatin dataset. The 10 colored curves in each graph denote the number of mice for every PDX.

[0093] FIG. **11**H illustrates the power curves at significance level $\alpha=0.05$ when the hazard ratio is between 0.1 and 0. 9 in OS analysis for the cisplatin dataset. The 10 colored curves in each graph denote the number of mice for every PDX.

DETAILED DESCRIPTION OF THE INVENTION

[0094] In the Summary of the Invention above and in the Detailed Description of the Invention, and the claims below, and in the accompanying drawings, reference is made to particular features (including method steps) of the invention. It is to be understood that the disclosure of the invention in this specification includes all possible combinations of such particular features. For example, where a particular feature is disclosed in the context of a particular aspect or embodiment of the invention, or particular claim, that feature can also be used, to the extent possible, in combination with and/or in the context of other particular aspects and embodiments of the invention, and in the invention generally.

[0095] The term "comprises" and grammatical equivalents thereof are used herein to mean that other components, ingredients, steps, etc. are optionally present. For example, an article "comprising" (or "which comprises") components A, B, and C can consist of (i.e., contain only) components A, B, and C, or can contain not only components A, B, and C but also one or more other components.

[0096] Where reference is made herein to a method comprising two or more defined steps, the defined steps can be carried out in any order or simultaneously (except where the context excludes that possibility), and the method can include one or more other steps which are carried out before any of the defined steps, between two of the defined steps, or after all the defined steps (except where the context excludes that possibility).

[0097] Where a range of value is provided, it is understood that each intervening value, to the tenth of the unit of the lower limit unless the context clearly dictate otherwise, between the upper and lower limit of that range and any other stated or intervening value in that stated range, is encompassed within the disclosure, subject to any specifically excluded limit in the stated range. Where the stated range includes one or both of the limits, ranges excluding either or both of those included limits are also included in the disclosure.

[0098] It will be appreciated that for simplicity and clarity of illustration, where appropriate, reference numerals have been repeated among the different figures to indicate corresponding or analogous elements. In addition, numerous specific details are set forth in order to provide a thorough understanding of the embodiments described herein. However, the embodiments described herein can be practiced without there specific details. In other instances, methods, procedures and components have not been described in detail so as not to obscure the related relevant function being described. Also, the description is not to be considered as limiting the scope of the implementations described herein. It will be understood that descriptions and characterizations of the embodiments set forth in this disclosure are not to be considered as mutually exclusive, unless otherwise noted.

[0099] A mouse clinical trial (MCT) is a population-based efficacy trial mimicking a human trial. It can be used to understand molecular mechanisms of drugs, to identify and prioritize indications, to reposition drugs, to guide clinical trials by discovering and evaluating biomarkers or assessing combination therapies. MCTs offer several advantages over human trials: reducing/removing much variance frequently encountered in human trials (e.g. prior treatments, individual health/nutrition conditions, other medications, heterogeneity in metabolisms and toxicity); less regulatory/ethic constraint

5

for scientific exploration; consistent drug exposure and reducing PK by using inbred mice; highly characterized PDXs with potentially historic data and high translatability; time saving and cost effective. The most distinct feature of MCTs is that PDX avatars of a single patient can join multiple treatment arms simultaneously, thus greatly enhancing the power of MCTs when properly designed and analyzed.

[0100] The present disclosure provides new methods for the design and analysis of both single-PDX studies and MCTs on a cohort of PDXs. In certain embodiments, the methods disclosed herein are based on an exponential growth model. Many mathematical models were proposed to describe tumor growth (Zhao et al., Clinical cancer research (2011) 17:1057-1064; Benzekry et al., PloS computational biology (2014) 10:e1003800), but might not be particularly advantageous in practice at the expense of requiring more parameters and data points. Furthermore, these models are largely unsuitable, or overly data-dependent, for data analysis in MCTs when tumor growth does not follow exponential kinetics, e.g. ones with V- or Λ-shapes. The major advantage of the exponential growth model lies in its simplicity, interpretability, and linearity after a logarithmic transformation, which is supported by our large collection of PDX trial datasets. In certain embodiment, the tumor growth rate k, and use k_T/k_C are calculated as an objective measure of tumor response to treatment. In certain embodiments, AUC ratio is used as a new tumor response endpoint superior to the conventionally used TGI. The AUC ratio is also suitable for immune-oncology pharmacology studies, in which large efficacy variations are observed. Defined as the median of ratios, this metric is in general not sensitive to extreme values and more robust than TGI.

[0101] In one aspect, the present disclosure provides a method for analyzing MCT data using AUC ratio, which is a measure of average growth rate ratio, and can be directly utilized to assess objective response rate (ORR). AUC ratio also measures accumulative tumor response even if a growth curve is not exponential.

[0102] In another aspect, the present disclosure provides a method for analyzing MCT data using linear mixed model (LMM). The LMM-based method can process nearly all MCT data, using quadratic terms of time if necessary. It can distinguish prognostic and predictive biomarkers, quantify different drug response of multiple cancers, and model heterogeneity of PDXs and mice.

[0103] In another aspect, the present disclosure provides a method for analyzing MCT data using additive frailty model. Like LMM, the additive frailty model takes into account of the frailty or heterogeneity of PDX's growth and drug response, as well as the clustering structure of PDXs and mice. Therefore, it gives more accurate estimate on hazard ratios and p-values than the proportional hazard Cox model, or the Kaplan-Meier method and the ordinary log-rank test.

[0104] The methods disclosed herein are not exclusive of each other, nor are they the only forms of corresponding analysis. In certain embodiments, the method uses a 2-level LMM by treating PDXs as the level-2 clusters and mice within PDX as the level-1 unit of analysis, where the dependent variable is the normalized AUC value. This is particularly suitable for irregular growth curves that cannot be satisfactorily modelled by the 3-level LMMs, without resorting to more complex methods like the piecewise

modeling approaches. It is also possible to jointly model the longitudinal and survival data. If there is no significant difference between PDX in drug response, the additive frailty model can be reduced to the shared frailty model. If a MCT is conducted at multiple sites, the method can use a 4-level LMM to capture the site variance should it not be negligible. Also, for the survival analysis, the definition of PFS and OS can vary by MCTs. For example, in leukemia PDXs, the end points can be defined as in human trials. Naturally, these methods can be used for single-PDX studies if the number of mice in each treatment group is sufficiently large.

[0105] In one embodiment, the method provides statistical power simulation using LMM that gives concrete recommendations on trial design. In particular, it answers the frequently asked question on how many PDXs and how many mice per PDX to use, and gives flexibility on the PDX and mouse number combinations. The power analysis results on both LMM and survival analysis advise cautions for using the "one mouse per PDX per treatment" paradigm, particularly in small scale MCTs. With proper adaption and extension, methods disclosed herein can make the design and analysis of MCTs more rational and more powerful.

[0106] In one aspect, the present disclosure provides a method of conducting mouse clinical trial comprising the steps of:

[0107] receiving a dataset of tumor volumes measured in a mouse clinical trial, wherein the mouse clinical trial comprises the steps of:

[0108] obtaining a tumor sample derived from a patient;

[0109] grafting the tumor sample to a treatment group comprising m mice and a control group comprising n mice, wherein m and n are integers;

[0110] administering a drug to the treatment group;

[0111] administering a vehicle to the control group; and

[0112] measuring tumor volume of the treatment group and tumor volume of the control group at a plurality of days;

[0113] determining tumor growth curve of the treatment group and tumor growth curve of the control group;

[0114] determining area under curve (AUC) of the treatment group (AUC_T) and AUC of the control group (AUC_C); and

[0115] evaluating efficacy of the drug based on an AUC ratio between the AUC_T and the AUC_C.

[0116] As used herein, "mouse clinical trial" refers to research studies that test how well new medical approaches work by using mice to mimic human diseases. In certain embodiments, the mice used mimic tumor. In certain embodiments, the mice used have patient derived xenograft (PDX). "Patient derived xenograft," as used herein, refers to a graft of tissue or cells taken from a human patient donor, and grafted into an animal model (e.g., mouse, rat, rabbit, etc.). In some embodiments, the xenograft tissue or cells are tumor tissue or cells, or cancerous tissue or cells. In some embodiments, the xenograft is pre-treated before grafting into the animal model. The term "pre-treated" when refers to tissue, generally relates to any processing methods known in the art to treat a tissue before its engraftment, such as washing, homogenization, re-suspension and mixing with a solution (e.g., saline, PBS etc.) or a matrix (e.g., collagen). The term "pre-treated" when refers to cells, includes any

processing methods known in the art to treat cells before its engraftment, such as culture, sub-culture, activating, treatment with an agent, centrifugation, re-suspension, filtration, and mixing with a solution (e.g., saline, PBS etc.) or a matrix (e.g., collagen). After grafted with xenograft, the animal model is allowed sufficient time to develop a lesion of the human disease for further use. The xenograft can be grafted to the animal model using any suitable methods known in the art, for example, by grafting cells subcutaneously, intraperitoneally, or intravenously through injection; or alternatively, by implanting a fraction of tissue through surgery. In some embodiments, the xenografts are tumor cells or cancerous cells, and are grafted to the animal model through subcutaneously injection.

[0117] As used herein, the term "tumor" or "cancer" refers to a group of diseases involving abnormal cell growth and division. In general, cancers can be categorized according to the tissue or organ from which the cancer is located or originated and morphology of cancerous tissues and cells. As used herein, cancer types include, without limitation, acute lymphoblastic leukemia (ALL), acute myeloid leukemia, adrenocortical carcinoma, anal cancer, astrocytoma, childhood cerebellar or cerebral, basal-cell carcinoma, bile duct cancer, bladder cancer, bone tumor, brain cancer, cerebellar astrocytoma, cerebral astrocytoma/malignant glioma, ependymoma, medulloblastoma, supratentorial primitive neuroectodermal tumors, visual pathway and hypothalamic glioma, breast cancer, Burkitt's lymphoma, ervical cancer, chronic lymphocytic leukemia, chronic myelogenous leukemia, colon cancer, emphysema, endometrial cancer, ependymoma, esophageal cancer, Ewing's sarcoma, retinoblastoma, gastric (stomach) cancer, glioma, head and neck cancer, heart cancer, Hodgkin lymphoma, islet cell carcinoma (endocrine pancreas), Kaposi sarcoma, kidney cancer (renal cell cancer), laryngeal cancer, leukaemia, liver cancer, lung cancer, neuroblastoma, non-Hodgkin lymphoma, ovarian cancer, pancreatic cancer, pharyngeal cancer, prostate cancer, rectal cancer, renal cell carcinoma (kidney cancer), retinoblastoma, Ewing family of tumors, skin cancer, stomach cancer, testicular cancer, throat cancer, thyroid cancer, vaginal cancer.

[0118] The term "tumor sample" or "cancer sample" used herein encompasses any sample obtained, directly or indirectly, from a tumor or cancer patient. A sample can, by way of non-limiting example, include cerebrospinal fluid (CSF), blood, amniotic fluid, sera, urine, feces, epidermal sample, skin sample, cheek swab, sperm, amniotic fluid, cultured cells, bone marrow sample and/or chorionic villi. Cancer cell cultures can also be used as samples. A cancer sample can also be, e.g., a sample obtained from any organ or tissue (including a surgical removal, biopsy or autopsy specimen), can comprise cells (whether primary cells or cultured cells), medium conditioned by any cell, tissue or organ, tissue culture. In some embodiments, biological samples suitable for the invention are samples which have been processed to release or otherwise make available a nucleic acid for detection as described herein. Suitable biological samples may be obtained from a stage of life such as a fetus, young adult, adult (e.g., pregnant women), and the like. Fixed or frozen tissues also may be used.

[0119] The "drug" used herein can be any chemical or medical approach that is tested in the mouse clinical trial. In certain embodiments, the drug used in the method is a potential drug for treating tumor or cancer. Examples of tumor/cancer drugs include, without limitation, Abritrexate, Afatinib dimaleate, Afinitor, Alecensa, Alectinib, Alimta, Araxane, Avastin, Bevacizumab, Blenoxane, Bleomycin, Camptosar, Capecitabine, Carboplatin, Ceritinib, Cetuximab, Cyramza, Docetaxel, Eloxatin, Erbitux, Erlotinib, Everolimus, 5-FU, Filotrif, Folex, Folex PFS, Fluorouracil Injection, Gefitinib, Gemcitabine Hydrochloride, Gemzar, Hydrea, Hydroxyurea, Iressa, Irinotecan hybdrochloride, Keytruda, Leucovorin Calcium, Lonsurf, Methotrxate, Methotrexate LPF, Mexate, Mexate-AQ, Mustargen, Navelbine, Necitumumab, Nivolumab, Opdivo, Osimertinib, Oxaliplatin, Paclitaxel, Panitumumab, Paraplat, Paraplatin, Pembrolizumab, Pemetrexed disoldium, Protrazza, Ramucirumab, Regorafenib, Stivarga, Tagrisso, Tarceva, Taxol, Taxotere, Trifluridine and Tipiracil ydrochloride, Vectibix, Wellcovorin, Xalkori, Xeloda, Zatrap, Ziv-aflibercept, Zykadia.

[0120] As used herein, a "vehicle" refers to a preparation that has no effect to treat the disease. Typically, the preparation does not include the drug being tested. In certain embodiments, the vehicle is a sham preparation (e.g., a placebo), either an excipient-only preparation or a sugar pill preparation.

[0121] As used herein, "administering" or "administration of" a drug or therapeutic to a subject (and grammatical equivalents of this phrase) includes both direct administration, including self-administration, directly into or onto a target tissue or to administer a therapeutic to a subject whereby the therapeutic positively impacts the tissue to which it is targeted, and indirect administration, including the act of prescribing a drug. The administration can be subcutaneous, intravenous, intramuscular, intra-articular, intra-synovial, intrasternal, intrathecal, intrahepatic, intraventricular, intragastrical, intralesional and intracranial injection or infusion techniques. In some embodiments, the drugs are administered intravenously, subcutaneously, orally, intramuscularly, intraventricularly, intragastrically, or by inhalation.

[0122] The term "tumor growth curve" used herein refers to an empirical model of tumor volume change over time. In certain embodiment, the tumor volume is measured every one, two, three or four days.

[0123] In certain embodiments, $AUC_T = \int_0^{d(T)} \ln V_x^{(T)} \, dx - d(T) \times \ln V_0^{(T)}$, wherein $V_0^{(T)}$ is the tumor volume of the treatment group at day 0, $V_x^{(T)}$ is the tumor volume of the treatment group at day x, d(T) is the number of days the measuring step for the treatment group lasts.

[0124] In certain embodiments, $AUC_C = \int_0^d \ln V_x^{(C)} \, dx - d \times \ln V_0^{(C)}$, wherein $V_0^{(C)}$ is $V_0^{(T)}$ the tumor volume of the control group at day 0, $V_x^{(C)}$ is the tumor volume of the control group at day x, d(C) is the number of days the measuring step for the treatment group lasts.

[0125] In certain embodiments, d(T)=d(C), wherein the

$$AUC \text{ ratio} = \frac{AUC_T}{AUC_C}.$$

[0126] In certain embodiments, d(T)≠d(C), wherein the

$$AUC\ \text{ratio} = \frac{AUC_T/d(T)^2}{AUC_C/d(C)^2}.$$

[0127] In certain embodiments, m≥3 and n≥3. In certain embodiments, m=n.

[0128] In certain embodiments, the evaluating step comprises determining that the drug is effective when the AUC ratio is less than 1.

[0129] In certain embodiments, the method disclosed herein further comprises the step of determining correlation of a factor to the efficacy of the drug. In certain embodiments, the factor is selected from the group consisting of: efficacy of the drug, cancer type of the patient, expression level of a gene, and existence of a mutation.

[0130] In certain embodiments, the factor is expression level of a gene. In one embodiment, the gene is EGFR and the drug is cetuximab.

[0131] In certain embodiments, the tumor volumes are between 100-300 mm^3.

[0132] In another aspect, the present disclosure provides a method of conducting mouse clinical trial comprising the steps of:

[0133] receiving a dataset of tumor volumes measured in a mouse clinical trial, wherein the mouse clinical trial comprises the steps of:

[0134] obtaining a tumor sample derived from a patient;

[0135] grafting the tumor sample to a treatment group comprising m mice and a control group comprising n mice, wherein m and n are integers;

[0136] administering a drug to the treatment group;

[0137] administering a vehicle to the control group; and

[0138] measuring tumor volume of the treatment group and tumor volume of the control group at a plurality of days;

[0139] evaluating impact of a factor on the tumor volume of the treatment group, wherein the tumor volume of the treatment group after logarithmic transformation has a linear relationship with the factor.

[0140] In certain embodiments, the factor is selected from the group consisting of: efficacy of the drug, cancer type of the patient, expression level of a gene, and existence of a mutation.

[0141] In one embodiment, the drug is cisplatin.

[0142] In certain embodiments, the cancer type is esophageal cancer, gastric cancer or lung cancer.

[0143] In once embodiments, the gene is ERCC.

[0144] In some embodiments, m≥3 and n≥3. In some embodiment, m=n.

[0145] In certain embodiments, the method disclosed herein further comprises conducting a second mouse clinical trial based on the impact of the factor determined in the evaluation step.

[0146] In yet another aspect, the present disclosure provides a method of conducting a mouse clinical trial, comprising

[0147] receiving a dataset of tumor volumes in a mouse clinical trial, wherein the mouse clinical trial comprises the steps of:

[0148] obtaining a plurality of tumor samples derived from a plurality of patients;

[0149] grafting the plurality of tumor samples to a treatment group of mice and a control group of mice;

[0150] administering a drug to the treatment group;

[0151] administering a vehicle to the control group; and

[0152] measuring tumor volume of the treatment group and tumor volume of the control group at a plurality of days;

[0153] determining progress-free survival (PFS) or overall survival (OS) of the treatment group and the control group;

[0154] evaluating efficacy of the drug based on the PFS or OS using an additive frailty model.

[0155] In certain embodiments, the additive frailty model includes a hazard function, wherein the hazard function for the j-th mouse of the i-th PDX is

$$h_{ij}(t) = h_0(t)\exp(u_i + (w + v_i)T_{ij} + \beta^T X_i)$$

wherein h_0 (t) is a baseline hazard function, u_i is a random effect associated with the i-th patient without drug treatment, w is mean drug effect, v_i is a random effect associated the i-th patient that depicts drug response deviating from w, T_{ij} is 0 for the control group and 1 for the treatment group, X_i is a vector for a covariate of the plurality of patients, β^T is a vector quantifying fixed effects of the covariate.

[0156] In certain embodiments, the PFS is the time until the tumor volume doubles.

[0157] In certain embodiments, the covariate is cancer type, expression of a gene or a gene mutation.

[0158] In certain embodiments, the treatment group consists of n mice for each patient and the control group consists of n mice for each patient, wherein n≥3.

[0159] In certain embodiments, the method disclosed herein further comprises conducting a second mouse clinical trial based on the hazard function.

[0160] As used herein, the term "gene" refers broadly to any nucleic acid associated with a biological function. Genes typically include coding sequences and/or the regulatory sequences required for expression of such coding sequences. The term gene can apply to a specific genomic sequence, as well as to a cDNA or an mRNA encoded by that genomic sequence. "Gene expression" refers to the process by which information from a gene is used in the synthesis of a functional product, including protein and functional RNA (e.g., tRNA, snRNA, and microRNA). In certain embodiments, the expression level of a gene can be measured by the transcript (e.g. mRNA) of the gene or the derivative thereof (e.g. cDNA).

[0161] In certain embodiments, N is between 20 and 80. In certain embodiments, N is about 30, 40, 50, 60, 70, 80, 90 or 100. In certain embodiments, N is around 50.

[0162] In certain embodiments, the gene expression profile described herein is obtained by transcriptome RNA sequencing or microarray. In certain embodiments, the gene expression profile described herein is obtained from the cancer genome atlas (TCGA) dataset.

[0163] In certain embodiments, the method described herein is computer-implemented, i.e., the method is carried out in a computer, e.g., a computer program executed by a CPU. A computer, as used herein, refers to a device (for general or specific purposes) that can be programmed to perform a set of arithmetic or logical operations automati-

cally. Computers, as used herein, include without limitation personal computers, workstations, servers, mainframes and supercomputers. The computer can be a stand-alone system, networked system or a virtual machine residing in a computing cloud. The methods described herein can be implemented with multithreading or other parallel computing methods.

[0164] The following examples are presented to illustrate the present invention. They are not intended to limiting in any manner.

EXAMPLE 1

[0165] This example shows that xenograft tumor growth largely follows exponential kinetics.

[0166] With an aim at developing new method of preclinical cancer pharmacology, we first set out to examine the growth patterns of xenograft tumors. Tumor grows by doubling of tumor cells, therefore, should follow exponential growth in theory. We thus began by testing actual PDX growth to see if it indeed follows exponential kinetics using our large pharmacology datasets of PDX trials. The exponential growth kinetics can be described by

$$V_x = V_0 e^{kx} \qquad (1)$$

where V_0 is the initial tumor volume normally ranging from 50-300 mm^3, V_x is the tumor volume at day x, k is a positive rate parameter. A logarithmic transformation on both sides of the above equation gives the linear equation

$$\ln V_x = \ln(V_0) + kx \qquad (2)$$

by which the estimate of k, termed $\hat{k}$, is obtained. The tumor volume doubling time (T_2) is then computed by

$$\frac{\ln(2)}{\hat{k}}.$$

Faster growing tumors have larger k and smaller T_2.

[0167] We applied Equation 2, by ordinary least square regression, to model tumor growth for 6310 PDX mice under vehicle treatment and had data for at least 5 days. Tumor volumes were usually measured every 3 to 4 days (twice weekly) before reaching 3000 mm^3. We found that the coefficient of determination (R^2) is >0.70 for nearly 100%, and >0.90 for 90% of the mice.

[0168] Tumor growth rates were found to vary within and between cancer types (FIG. 1). The median T_2 ranges from 8.0 days in liver cancer and breast cancer to 13.1 days in head and neck cancer, and significant difference is seen across the 10 cancer types with at least 4 PDXs (one-way ANOVA p-value=0.002). Within a cancer type, T_2 ranges from about 2-fold in gallbladder cancers and ovarian cancers to about 6-fold in colorectal cancers and lung cancers. The average T_2 across all PDXs is 9.8±4.8 days.

[0169] Tumor growth rate also varies among the mice within a PDX model. The coefficient of variation for T_2 is 0.29±0.12 (mean±SD), ranging from to 0.07 to 0.74, for PDXs with data for at least 5 mice. The coefficient of variation reduces to 0.20±0.09, ranging from 0.03 to 0.74, when calculated by individual projects, under which mice of a PDX were implanted with segments of the same tumor chunk, treated and monitored in the same experimental condition. Thus, a significant portion of the growth variation should stem from tumor heterogeneity. In summary, under

vehicle treatment, most PDX tumors exhibit exponential growth until tumor volume reaches between 2000-3000 mm^3.

EXAMPLE 2

[0170] This example illustrates drug treatment causes complex growth kinetics in PDXs.

[0171] We next examined tumor growth kinetics under various drug treatments. We examined growths of 27771 PDX mice, and found that tumor shrunk for at least one measurement day in 26.0% of them, though some might result from measurement error. At termination point, tumor volume ratio (V_e/V_0) of end tumor volume (V_e) versus dosing starting volume (V_0) are found to be 0% (2.0% of mice), <100% (10.8% of the mice), ~100% (~5% of the mice), <173% (19.8% of mice), <200% (22.8% of mice). Studies also ran longer in drug groups (29.7±14.8 days) than in vehicle groups (24.0±9.1 days).

[0172] We then attempted to assess whether tumor growth still follows exponential kinetics under drug treatment. In general, a more potent drug led to smaller tumors at the end of a study. There was a relationship between the regression R^2 and V_e/V_0, the ratio between the ending and starting tumor volumes (FIG. 2). The average R^2 was smallest when V_e/V_0 was ~1, as expected mathematically, and R^2 increased quickly when V_e/V_0 went down and up. The percentage of growth curves with $R^2>0.70$ was 91.8%, 95.1%, and 96.3% when V_e/V_0 was larger than 2, 3, and 4, respectively. If $V_e/V_0<0.5$, about 70% of growth curves had $R^2>0.70$. Therefore, under drug treatment, most tumors either did not grow (or shrink) much, or grew (or shrink) exponentially that can be well modeled by Equations (1) and (2).

[0173] Overall, around 20% of growth curves under drug treatment were not exponential, as suggested by a clustering analysis (FIG. 3A). Indeed, when Equation 2 was used to model tumor growth, we found that R^2 is >0.70 for 80% of the growth curves. However, only about 8% of tumors had non-exponential growth curves with $V_e/V_0>2$ or <0.5 (FIG. 3B). Among them, 10-20% had irregular shapes, the remaining had V-like and A-like shapes. The former might suggest development of drug resistance and the latter a latent period before drug effect took place. Overall, tumor growth under treatments displayed more complex kinetic patterns as compared to no treatment.

EXAMPLE 3

[0174] This example illustrates that TGI is a tumor response endpoint biased by tumor growth rate and time of study termination.

[0175] We next investigated Tumor Growth Inhibition (TGI), a commonly used tumor response endpoint, and its variants or equivalent end points, to determine its adequacy for pharmacology evaluation. TGI is defined as

$$TGI = 1 - \frac{\Delta T}{\Delta C} = 1 - \frac{V_x^{(T)} - V_0^{(T)}}{V_x^{(C)} - V_0^{(C)}} \qquad (3)$$

where $V_x^{(T)}$ and $V_0^{(T)}$ are the tumor volume at day x and day 0 in the drug treatment group; $V_x^{(C)}$ and $V_0^{(C)}$ are the corresponding volumes in the vehicle or control group. TGI and $\Delta T/\Delta C$ equivalently used in practice, and frequently

presented in percentage. Usually, there are multiple mice in both drug and vehicle groups, so these 4 tumor volume parameters are the averages or medians. By definition, if there is no response, then TGI=0. If a drug causes tumor growing faster than vehicle, then TGI<0. If tumor growth is inhibited by treatment, then TGI>0; if the tumor volume does not change, then TGI=1, and if the tumor shrinks, i.e. $0 \leq V_x^{(T)} < V_0^{(T)}$, then TGI>1.

[0176] To assess the time-dependency of TGI, we assumed that tumor grows exponentially in both drug and vehicle groups with rate constants k_T and k_C, respectively, and with equal starting volumes, i.e. $V_0^{(T)} = V_0^{(C)}$, then

$$TGI = 1 - \frac{e^{k_T x} - 1}{e^{k_C x} - 1} \quad (4)$$

In our PDX data, k_C ranges from 0.0139 to 0.307, and k_T ranges from −0.488 to 0.273. The rate ratio k_T/k_C is a constant that measures drug response, if both groups grow exponentially. For example, if $k_T/k_C=0.5$, then a drug inhibits tumor growth by half, so that it takes twice the time to double the tumor volume under drug than vehicle treatment. The smaller the ratio is, the more potent the drug is. A negative k_T/k_C value indicates tumor shrinkage under drug treatment.

[0177] Drug should almost always inhibit tumor growth, therefore, $k_T \leq k_C$ and TGI>0. We plotted TGI values against days-post initial dosing for the first 60 days, when 99.5% of our studies ended (FIGS. 4A-C). With k_T/k_C as a tumor response measurement, we observed: 1) TGI is time-dependent for any given k_T/k_C value. If TGI>1, its value goes down toward 1 with time; if 1>TGI>0, its value goes up toward 1 with time, even more so for faster growing tumors; 2) TGI is dependent on tumor growth rate (k_C). For a given k_T/k_C, TGI at a fixed time was larger for faster growing (larger k_C) tumors if between 0 and 1, and smaller if >1.

[0178] We then tested the above theoretical predictions by examining a MCT dataset consisted of 40 PDXs with 3:3 design format (3 mice in treatment/3 in vehicle groups for each PDX). Tumor volumes were measured at day 0, 3, 7, 10, 14, 17, and 21. The average starting tumor volumes $V_0^{(T)}$ and $V_0^{(C)}$ were between 115 mm³ and 194 mm³, and for a PDX, $V_0^{(T)}$ and $V_0^{(C)}$ differ by 47% on average. We found that the first two TGIs at day 3 and 7 frequently behave irregularly, likely caused by the initial unstable response to drug treatment and the relatively large measurement errors when tumors are small (FIG. 5A). Thereafter, TGIs varied with time as expected in about 90% PDXs. The drug was very potent, 39 PDXs showed certain level of response, and tumor shrunk in 2 PDXs. We found strong positive correlations between k_C and TGIs at day 14, 17 and 21 (FIGS. 5B-D) for 24 PDXs with all TGIs between 0 and 1. The correlation at day 21 became weaker because TGIs for many PDX were getting close to 1. In another MCT dataset of 38 PDXs, we observed strong negative correlations between k_C and TGIs for 18 PDXs 4 measurement days when TGI is larger than 1 (FIGS. 5E-5F).

[0179] TGI as tumor response readout may have other drawbacks. First, in the above analysis, we stipulated $V_0^{(T)} = V_0^{(C)}$, or that tumors are in the same growth phase when dosing starts. In practice, however, it is not always possible to ensure such matching, especially when the number of mice for a PDX is small, which could affect TGI values

dramatically. For example, if $V_0^{(T)}=\frac{1}{2}V_0^{(C)}$, then a TGI originally being 0.5 becomes 0.75. Secondly, tumor volumes, consequently TGIs, may fluctuate irregularly from day to day, especially in drug treatment groups. It is difficult to determine which day's TGI should be used. Thirdly, it is a common practice to use TGI from the same day for comparison, however, it may not be available for some fast growing tumors. These inflexibilities of TGI, in addition to its inherent inaccuracy, may limit its application as a tumor response readout.

[0180] There are some alternative definitions of TGI, notably

$$TGI = 1 - \frac{V_x^{(T)}}{V_x^{(C)}} \text{ and } TGI = 1 - \frac{V_x^{(T)}/V_0^{(T)}}{V_x^{(C)}/V_0^{(C)}}.$$

The terms

$$\frac{V_x^{(T)}}{V_0^{(T)}} \text{ and } \frac{V_x^{(C)}}{V_0^{(C)}}$$

are the relative tumor volumes. Assuming tumor grows exponentially in both drug and vehicle groups, these two definitions reduce to

$$TGI = 1 - \frac{V_0^{(T)} e^{k_T x}}{V_0^{(C)} e^{k_C x}} \text{ and } TGI = 1 - \frac{e^{k_T x}}{e^{k_C x}},$$

which become equivalent if $V_0^{(T)}=V_0^{(C)}$. We found that they were more sensitive in their dependence on time and growth rate than TGI defined in Equation 3 (FIGS. 6A-C).

EXAMPLE 4

[0181] This example illustrates that AUC ratio is an unbiased metric based on k_T/k_C measuring tumor response with superiority to TGI

[0182] We mentioned in EXAMPLE 3 that k_T/k_C is a constant measuring tumor response under the exponential growth assumption. By Equation 2, it is easy to show that

$$\frac{k_T}{k_C} = \frac{\int_0^d \ln V_x^{(T)} dx - d \times \ln V_0^{(T)}}{\int_0^d \ln V_x^{(C)} dx - d \times \ln V_0^{(C)}} = \frac{AUC_T}{AUC_C} \quad (5)$$

The two starting tumor volumes, $V_0^{(T)}$ and $V_0^{(C)}$, need not to be the same. These two AUCs (area under curve) are illustrated in (FIG. 7A), and the AUC ratio equals k_T/k_C. If a study stops at different time for the two groups, d_T for the drug group and d_C for the vehicle group, we need to normalize the AUCs by d_T^2 or d_C^2. For convenience, we still call the normalized AUC as AUC, and the ratio between the two normalized AUCs as the AUC ratio:

$$\frac{k_T}{k_c} = \frac{AUC_T/d_T^2}{AUC_C/d_C^2} \quad (6)$$

A smaller AUC ratio indicates better drug efficacy. When the ratio is negative, tumor shrinks under drug treatment; when the ratio is larger than 1, tumor grows faster under drug treatment.

[0183] We can use the trapezoidal rule to obtain AUCs from the growth curves, even when they are non-exponential, for which AUC is a measure of average drug effect during study period. Similar to TGI, AUC ratio varies more in the first week(s) before reaching stable response. Unlike TGI that approaches 1 with time, AUC ratio converges to a value, which is k_T/k_C under exponential growth kinetics, and which may be far away from 1 (FIGS. 7B-7C).

[0184] For multiple mice in drug group (n_T) and vehicle group (n_C), AUCs in each group can be viewed as random samplings from corresponding normal distributions with sizeable standard deviations against the corresponding mean. The two normal distributions can differ in both mean and standard deviation. AUC ratio, therefore, follows a Cauchy-like distribution with heavy tails (Hinkley D V, Biometrika (1969) 56(3):635-39), where the median of ratios is a better metric than the ratio of medians (Brody J P et al., PNAS (2002) 99(20):12975-8). We computed the $n_T \times n_C$ AUC ratios, then take their median to calculate the median of ratios.

[0185] To calculate the ratio of medians, we first computed the median of the n_T AUCs and the median of the n_C AUCs, then took their ratio. All AUC ratios in the tables and graphs, unless specified otherwise, were obtained by the median-of-ratios method.

[0186] We used a bootstrap procedure to obtain the confidence interval (CI) of AUC ratio. Specifically, we performed a random sampling with replacement to get n_T AUCs from drug group and n_C AUCs from vehicle group, then calculated median AUC ratio. This procedure was repeated 1000 times to get a list of median AUC ratios, from which an equitailed 90% confidence intervals was constructed. The distribution of the median AUC ratio was often non-normal and skewed due to small number of mice and diverse drug response, under which the bootstrap confidence intervals were usually much tighter than ones calculated by formulas based on normal distribution, e.g., $\bar{x} \pm 1.96SE(\bar{x})$ for the 95% confidence interval. The bootstrap confidence interval got smaller when mice had more similar tumor growth curves.

[0187] We further investigated how number of mice affects estimate error of the median AUC ratio. For simplicity, we assumed a balanced design with equal number of mice in the two groups (n:n design), and we estimated the bootstrap CI widths. From a MCT study with 50 PDXs and with 10 mice each in vehicle group and drug group, we calculated the 90% bootstrap confidence interval of the AUC ratios, and we found that the 1:1 design has very large CI width. Having more than one mouse per PDX model substantially reduced the CI width. 3:3 and up designs appeared to be a reasonable balance of measurement accuracy and cost for this specific case (FIG. 7D). Similar observations were seen in several other MCTs (FIGS. 7 E-H).

[0188] Our results show that the AUC ratio gives great flexibility for studies: mice can be enrolled as long as tumor volumes are between 100-300 mm^3, and there is no need to match starting tumor volumes between a drug group and a vehicle group. Studies can be stopped at different time for different PDXs, suited to their tumor growth rates, and drug efficacy is calculated using tumor volumes from nearly any time. If a drug has good efficacy, the drug group can run longer than the vehicle group to get better characterization of its efficacy and response profile, besides getting more accurate AUC ratio. Mice for a PDX can have very different growth rates, in a drug or in vehicle group, which can all be captured by individual AUCs. In summary, AUC ratio displays significant operational robustness, in addition to accuracy, as compared to TGI.

EXAMPLE 5

[0189] This example illustrates methods for MCT data analysis using the AUC ratio.

[0190] A MCT, similar to a phase-2 human clinical trial, is a population based investigation where tumor response rate (RR) and survival parameters are two standard efficacy readouts. Unlike human studies, a MCT can have multiple arms (vehicle, comparator arms, dosages, etc.) in which a given PDX can present simultaneously and each PDX model maybe represented by multiple mice. In other words, conceptually, a cancer patient simultaneously participates multiple arms and has replicates in each arm. This makes MCT a powerful preclinical tool. However, there is a need for new methods to support MCT data analysis that are different from those for individual preclinical studies and also those for human trials. The following describes cases assessing the correlation of EGFR gene expression to gastric PDX response to cetuximab using the AUC ratio.

[0191] We previously described a MCT study involving a cohort of 20 gastric PDXs where EGFR overexpression seems associated with positive response to cetuximab PDXs based on TGI type of response endpoint (Zhang L et al., Scientific Reports (2013) 3:2992). We expanded the studies to 27 PDXs, completed at the different times with other study variations: mouse numbers per arm (3-10 in a drug or vehicle group), durations (14-63 days), etc. We calculated TGIs at day 14, and also AUC ratios using full set of data for all 27 PDXs. We observed a much stronger correlation between EGFR mRNA levels and the AUC ratios ($R^2=0.45$, p-value=1.1×10^{-4}, FIG. 8A), than between EGFR level and TGIs ($R^2=0.17$, p-value=0.03, FIG. 8B). The most responsive GA0152 had extremely high EGFR expression (FPKM>1000). Furthermore, for the 7 PDXs with high EGFR levels (FPKM around or larger than 20), 6/7 experienced tumor volume reduction under treatment, with only exception of GA2140 that was the third most resistant. GA2140 carries EGFR L435R (Ensemble ENST00000455089) missense mutation, predicted to be disruptive to protein function by SIFT(37), and might be a biomarker for cetuximab resistance. This analysis also supports that AUC is more robust tumor response readout over TGI in MCT and particularly for biomarker discovery. Our observation that EGFR over-expression is a predictive biomarker to cetuximab is supported by a phase 2 trial and a phase 3 trial with data re-interpretation (Zhang X et al., Medical Oncology (2014) 31(10):226). Specifically, we found that for patient with IHC score greater than ~200, the 7 patients receiving cetuximab in addition had significantly longer PFS (8.1±6.1 months, one-sided Mann-Whitney U-test p-value=0.03) and OS (19.5±12.0 months, p-value=0. 02) than the 19 patients receiving only chemotherapies

(PFS=4.1±3.2 months, OS=10.1±7.8 months). Two censored patients with very low OS and PFS in the chemotherapy group were excluded from the analysis.

EXAMPLE 6

[0192] This example illustrates methods for MCT data analysis using linear mixed models.

[0193] In a MCT, tumor volume is measured at multiple time points for each mouse, and these tumor volumes are often correlated, as in a typical longitudinal study. As shown above, almost all growth curves under vehicle treatment can be modeled by the linear Equation 2, and under drug treatment, about 80% of the growth curves are linear or close to linear. If we introduce a quadratic term on the day (x^2), more than 90% of the growth curves can be fitted with $R^2>0.7$, and 97% with $R^2>0.4$. With such strong linearity, the linear mixed models (LMM) is a proper and powerful tool to analyze the clustered longitudinal data from MCTs (West B T et al., "Linear Mixed Models: A Practical Guide Using Statistical Software, Second Edition", Crc Press (2014)). Specifically, a 3-level model is appropriate, in which PDX and mouse are random factors, and covariates at the PDX-level and mouse-level can be included (FIG. 9A). We used an MCT to illustrate the application of LMMs for drug response evaluation and biomarker discovery.

[0194] The MCT evaluated cisplatin response (4 mg/kg, daily dosing for 3 weeks) on 42 PDXs including 13 esophageal cancers (ES), 21 gastric cancers (GA) and 8 lung cancers(LU), each PDX had 5-9 mice (FIGS. 9B-C). A general model was specified for tumor volume, in log scale, at day t for mouse i within PDX j as follows:

$$\ln V_{tij} = \beta_0 + \beta_1 \times Day_t + \beta_2 \times Day_t \times CancerTypeGA_j + \tag{7}$$
$$\beta_3 \times Day_t \times CancerTypeLU_j + \beta_4 \times Day_t \times Treatment_{ij} +$$
$$\beta_5 \times Day_t \times CancerTypeGA_j \times Treatment_{ij} +$$
$$\beta_6 \times Day_t \times CancerTypeLU_j \times Treatment_{ij} +$$
$$u_{0j} + u_{1j} \times Day_t + u_{(0i|j)} + u_{(1i|j)} \times Day_t + \varepsilon_{tij}$$

[0195] The model used vehicle in ES as the reference. There were 6 fixed effects, β_0 for the intercept, β_1 for the time slope, β_2 and β_3 quantify the growth rate difference of GA and LU with respect to ES, β_4 measures cisplatin effect, β_5 and β_6 check if GA and LU respond differently to cisplatin. The model also had 5 random effects, including the residual ϵ_{tij}. In a MCT, we can view the cohort of PDXs as random samples from a PDX or patient population, therefore, they have different growth rates, which is modeled by the random effect u_{1j} associated with the time slope. Similarly, we model the growth difference for mice within a PDX by the random effect $u_{1i|j}$. Mice and PDX may also have different starting tumor volumes, which are modeled by the two random effects on intercept: u_{0j} and $u_{0i|j}$. Therefore, our LMM captures both PDX-level and mouse-level growth heterogeneity under vehicle and drug treatments. From the modeling fitting (Table 1), we observe that (1) tumor in GA grows slightly faster than ES, while tumor growth is much faster in LU than in ES and GA; (2) cisplatin caused comparable responses on the 3 cancer types (p-values for β_5 and β_6 are >0.05). From the model, we can get fitted cancer specific growth curves, as well as PDX and mouse specific

growth curves. On average, cisplatin reduces tumor growth rate by about 38%. The AUC ratio method gives a close 36%.

TABLE 1

Parameters estimated for the LMM (Equation 7) of the cisplatin dataset

Fixed-Effect Parameters	Estimate*	p-value
β_0 (Intercept)	5.2641(0.0257)	0
β_1 (Day)	0.0605(0.0043)	1.5E−43
β_2 (Day × CancerTypeGA)	0.0091(0.0055)	0.098
β_3 (Day × CancerTypeLU)	0.0297(0.0071)	2.8E−5
β_4 (Day × Treatment)	−0.0282(0.0031)	1.2E−19
β_5 (Day × CancerTypeGA × Treatment)	0.0037(0.0039)	0.35
β_6 (Day × CancerTypeLU × Treatment)	−0.0011(0.0052)	0.84

*parameters estimated by the REML method in the R nlme package.

[0196] The LMM can readily incorporate PDX-level genomic covariates, e.g. gene expression and mutation, for biomarker analysis. We used the same dataset to examine if ERCC1 expression is related to cisplatin response in gastric cancer by fitting the following LMM:

$$\ln V_{tij} = \beta_0 + \beta_1 \times Day_t + \beta_2 \times Day_t \times ERCC1_j + \beta_3 \times Day_t \times$$
$$Treatment_{ij} + \beta_4 \times Day_t \times ERCC1_j \times Treatment_{ij} + u_{0j} +$$
$$u_{1j} \times Day_t + u_{(0i|j)} + u_{(1i|j)} \times Day_t + \epsilon_{tij} \tag{8}$$

[0197] In this model, β_2 evaluates ERCC1 expression as a prognostic biomarker since it is for both vehicle and cisplatin groups. The fitted value of β_2 is −0.0155, indicating that higher expression of ERCC1 leads to slower tumor growth (FIG. 9E). The coefficient β_4 examines ERCC1 expression as a predictive biomarker for cisplatin. The fitted value of β_4 is 0.0136, close to that of β_2. Therefore, high ERCC1 expression acts adversely to cisplatin treatment (FIG. 9E). The parameter β_3 quantifies cisplatin treatment and is estimated to be −0.0879. Results from our LMM may have clinical implications.

[0198] Our results indicates that patients with lower ERCC1 expression are likely to have worse tumor progression but also benefit more from cisplatin and likely other platinum-based chemotherapies. These two effects work against each other and might be in comparable magnitude. Accordingly, it is hard to evaluate ERCC1 expression as a predictive biomarker in relevant clinical trials when PFS and OS are used as end points. Indeed, controversial trial conclusions exist. While more trials claim that patients benefit from low ERCC1 expression (Metzger R et al., J Clinical Oncology (1998;) 16(1):309-16; Kwon H C et al., Annals of Oncology (2007) 18(3):504-9; Hirakawa M et al., Cancer Chemotherapy and Pharmacology (2013) 71(3):789-97; Miura J T et al., Cancer Biology & Therapy (2015) 16(5): 764-9), there are some stating that overexpression of ERCC1 is related to longer survival (Bamias A et al., Cancer Chemotherapy & Pharmacology (2010) 65(6):1009-21; Baek S K et al., Cancer Research & Treatment (2006) 38(1):19-24; Kim K H et al., Biomarkers (2011) 16(1):74-82). Still others found no connection (Sonnenblick A et al., Medical Oncology (2012) 29(5):3035-8). In one study, the researchers found that high ERCC1 expression is associated with decreased OS in chemotherapy but with increased OS in patients with surgery alone (Squires M H et al., Cancer (2013) 119(17):3242-50). Our MCT supports the notation that patients with low ERCC1 benefit more from cisplatin chemotherapy.

[0199] The LMM uses all tumor volume data, even if some mice may have less data points than others. We performed a power analysis based on parameters estimated from fitting the cisplatin dataset by a simple LMM:

$$\ln V_{tij} = \beta_0 + \beta_1 \times \mathrm{Day}_t \beta_2 \times \mathrm{Day}_t \times \mathrm{Treatment}_{ij} + u_{0j} + u_{1j} \times \mathrm{Day}_t + u_{(0ij)} + u_{(1ij)} \times \mathrm{Day}_t + \epsilon_{tij} \quad (9)$$

[0200] We assumed n:n designs so that for each PDX, there were n mice in the vehicle group and n mice in the drug group. The MCT run for 3 weeks, and all mice had tumor volume data for 7 measurement days including day 0. At significance level $\alpha=0.05$, we obtained power curves by simulations for $\beta_1/\beta_2=-0.1$ to -0.9, that is, the drug treatment reduces tumor growth rate by 10% to 90% (FIGS. 9F-9G). We observed 1) the 1:1 design had much weaker power than any design with more than one mouse per PDX (n>1); and 2) power increased quickly from 1:1 design to 2:2 design, and from 2:2 design to 3:3 design, after that, the increase slowed down significantly. Therefore, having 3 or more mice per PDX per treatment can give MCTs adequate power with a much smaller number of PDXs.

[0201] Next, we attempted to use power curves to guide MCT design. We set to perform a hypothetic MCT on multiple cancer types to prioritize indications for future human trials. We stipulated a 20% efficacy difference as the selection threshold. Per FIG. 9E, we can conduct MCT by one of the following enrolling schemes to achieve 0.05 significance level and 90% power: 1) 35 PDXs for each cancer type and each PDX with one mouse; 2) 20 PDXs for each cancer type and each PDX with 2 mice; 3) 13 PDXs each with 3 mice, 4) 10 PDXs for each cancer type and each PDX with 4 mice, and so on. This gives flexibility in operations, especially when the availability of PDXs and mice is constrained.

EXAMPLE 7

[0202] This example illustrates methods for MCT data analysis using additive frailty models.

[0203] Survival analysis are the most important endpoints of human clinical trials and can also be potentially adapted to MCT by first defining "clinical endpoint" of PFS (progress-free survival) and OS (overall survival) in preclinical setting. By the RECIST standard (Therasse P et al., J Natl Cancer Inst (2000) 92(3):205-16), we define PFS as the time until the starting tumor volume increases by 73%, and define OS as the time until the starting tumor volume triples, at which the tumor volume is usually between 300-600 mm³, depending on initial tumor volumes. As we have shown in examples above, tumors already start exponential growth before it reaches 600 mm³. The definitions are more of a custom and can certainly be adjusted otherwise. For example, Gao et al defined PFS as the time until tumor volume doubles (Gao H et al., Nat Med (2015) 21(11):1318-25). We can also define OS as the time until the starting tumor volume quadruples and so on.

[0204] In human oncology trails, survival time of patients is usually assumed to be independent of each other. In MCT, this assumption does not hold. Mice have correlated survival time both within a PDX and between treatments (FIGS. 10A-B). There is heterogeneity on hazard and drug response for PDXs. We used an additive frailty model to fit the survival data in MCTs (Rondeau V et al., J Statistical Software (2012) 47(4):1-28; Hanagal D D, Statistical Meth-

ods in Medical Research (2015) 24(6):936-36). In this model, the hazard function for the j-th mouse of the i-th PDX is

$$h_{ij}(t) = h_0(t) \exp(u_i + (w + v_i)T_{ij} + \beta^T X_i)$$

where $h_0(t)$ is the baseline hazard function. Parameter u_i is the random effect (the first frailty term) associated with the i-th PDX that captures its characteristic growth, thus survival behavior, without drug treatment. Parameter v_i is the random effect (the second frailty term) associated the i-th PDX that depicts its drug response deviating from the mean drug effect w of all PDXs. T_{ij} is the treatment variable and it equals 0 for the vehicle treatment and 1 for the drug treatment; X_i is a vector for the PDX's covariates, e.g., cancer type and gene expression; β^T is the parameter vector quantifying the fixed effects of the covariates. The two random effects u_i and v_i assume a bivariate normal distribution with zero means, variance σ^2 and τ^2, and covariance $\rho\sigma\tau$. If the two random effects u_i and v_i are removed, the model reduces to the proportional hazard Cox model.

[0205] We used the cisplatin dataset in the previous example to illustrate modeling by the additive frailty model, using the R package frailtypack (Rondeau V et al., J Statistical Software (2012) 47(4):1-28). For simplicity, we used treatment as the sole covariate. By Equation 10, we observed that both frailty terms are significant larger than 0 (Wald test p-value<0.05) for PFS and OS analyses. Therefore, there is strong heterogeneity among PDXs and their drug response. The hazard ratio (HR) is estimated to be 0.40 (95% CI: 0.31-0.50) for PFS and 0.21 (95% CI: 0.15-0.31) for OS, both are sizably smaller than estimations under the proportional hazard Cox model, which gives PFS HR=0.48 (95% CI: 0.40-0.58) and OS HR=0.36 (95% CI: 0.28-0.46) (FIGS. 11A-B). These results show that without considering PDX heterogeneity, the drug effect can be severely underestimated.

[0206] The first frailty term u_i for a PDX measures its hazard of tumor progression. We observed that the estimated frailties from the OS survival analysis are negatively correlated with PDXs' growth rates in the vehicle group (R²=0.85, FIG. 11C). The fitting is much loose for the PFS survival analysis (R²=0.39, FIG. 11D), which can be explained by the somewhat irregular tumor growth compounded by relatively large measurement error at small tumor volumes.

[0207] We performed statistical power analysis for the survival analysis by assuming the n:n designs, and using parameters estimated from the cisplatin dataset with Weibull hazard functions (FIGS. 11E-H). We found that the survival analysis generally has lower power than LMM for comparable drug efficacy, and the 3:3 or above designs generally give much more power than the 1:1 and 2:2 designs.

[0208] The additive frailty model can readily be used for biomarker assessment and discovery by incorporating genomic status (e.g., mutation or expression) as a covariate. Because the frailty term already extracts PDX heterogeneity, the frailty model can be more accurate on quantifying the effect of a potential biomarker. Compared to LMM, survival analysis does not assume exponential or other forms of growth curves, and is therefore more flexible.

REFERENCES

[0209] 1. Povlsen C O, Rygaard J. Heterotransplantation of human adenocarcinomas of the colon and rectum to the mouse mutant Nude. A study of nine consecutive trans-

plantations. Acta pathologica et microbiologica Scandinavica Section A, Pathology 1971; 79(2):159-69.

[0210]   2. Castro J E. Human tumours grown in mice. Nature: New biology 1972; 239(90):83-4.

[0211]   3. Cobb L M. The behaviour of carcinoma of the large bowel in man following transplantation into immune deprived mice. British journal of cancer 1973; 28(5):400-11.

[0212]   4. Rosfjord E, Lucas J, Li G, Gerber H P. Advances in patient-derived tumor xenografts: from target identification to predicting clinical response rates in oncology. Biochemical pharmacology 2014; 91(2):135-43.

[0213]   5. Hidalgo M, Amant F, Biankin A V, Budinska E, Byrne A T, Caldas C, et al. Patient-derived xenograft models: an emerging platform for translational cancer research. Cancer discovery 2014; 4(9):998-1013.

[0214]   6. Gao H, Korn J M, Ferretti S, Monahan J E, Wang Y, Singh M, et al. High-throughput screening using patient-derived tumor xenografts to predict clinical trial drug response. Nature medicine 2015; 21(11):1318-25.

[0215]   7. Owonikoko T K, Zhang G, Kim H S, Stinson R M, Bechara R, Zhang C, et al. Patient-derived xenografts faithfully replicated clinical outcome in a phase II co-clinical trial of arsenic trioxide in relapsed small cell lung cancer. Journal of translational medicine 2016; 14(1):111.

[0216]   8. Guo S, Qian W, Cai J, Zhang L, Wery J P, Li Q. Molecular pathology of patient tumors, patient derived xenografts and cancer cell lines. Cancer research 2016.

[0217]   9. Tentler J J, Tan A C, Weekes C D, Jimeno A, Leong S, Pitts T M, et al. Patient-derived tumour xenografts as models for oncology drug development. Nat Rev Clin Oncol 2012; 9(6):338-50.

[0218]   10. DeRose Y S, Wang G, Lin Y C, Bernard P S, Buys S S, Ebbert M T, et al. Tumor grafts derived from women with breast cancer authentically reflect tumor pathology, growth, metastasis and disease outcomes. Nature medicine 2011; 17(11):1514-20.

[0219]   11. Zhang X, Claerhout S, Prat A, Dobrolecki L E, Petrovic I, Lai Q, et al. A renewable tissue resource of phenotypically stable, biologically and ethnically diverse, patient-derived human breast cancer xenograft models. Cancer research 2013; 73(15):4885-97.

[0220]   12. Zhao X, Liu Z, Yu L, Zhang Y, Baxter P, Voicu H, et al. Global gene expression profiling confirms the molecular fidelity of primary tumor-based orthotopic xenograft mouse models of medulloblastoma. Neuro-oncology 2012; 14(5):574-83.

[0221]   13. Kabos P, Finlay-Schultz J, Li C, Kline E, Finlayson C, Wisell J, et al. Patient-derived luminal breast cancer xenografts retain hormone receptor heterogeneity and help define unique estrogen-dependent gene signatures. Breast cancer research and treatment 2012; 135(2): 415-32.

[0222]   14. Julien S, Merino-Trigo A, Lacroix L, Pocard M, Goere D, Mariani P, et al. Characterization of a large panel of patient-derived tumor xenografts representing the clinical heterogeneity of human colorectal cancer. Clinical cancer research an official journal of the American Association for Cancer Research 2012; 18(19):5314-28.

[0223]   15. Malaney P, Nicosia S V, Dave V. One mouse, one patient paradigm: New avatars of personalized cancer therapy. Cancer letters 2014; 344(1):1-12.

[0224]   16. Smith P G, Sutton D, Bertotti A, Trusolino L, Airhart S, Ming S T, et al. Abstract 1191: Translational Proof-of-Concept (TransPoC), a not-for-profit research organization enabling access to large-scale translational oncology platforms: The Patient-Derived Xenograft network. Cancer research 2014; 74(19 Supplement):1191-91.

[0225]   17. Budinská E, Popovici V. The EurOPDX consortium: Sharing patient tumor-derived xenografts for collaborative multicentric preclinical trials. Molecular cancer therapeutics 2014; 12(11_Supplement): A8-A8.

[0226]   18. Chen D, Huang X, Cai J, Guo S, Qian W, Wery J P, et al. A set of defined oncogenic mutation alleles seems to better predict the response to cetuximab in CRC patient-derived xenograft than KRAS 12/13 mutations. Oncotarget 2015; 6(38):40815-21.

[0227]   19. Guo S, Chen D, Huang X, Cai J, Wery J P, Li Q X. Cetuximab response in CRC patient-derived xenografts seems predicted by an expression based RAS pathway signature. Oncotarget 2016.

[0228]   20. Guo S, Qian W, Cai J, Zhang L, Wery J P, Li Q X. Molecular Pathology of Patient Tumors, Patient-Derived Xenografts, and Cancer Cell Lines. Cancer research 2016.

[0229]   21. Zhang L, Yang J, Cai J, Song X, Deng J, Huang X, et al. A subset of gastric cancers with EGFR amplification and overexpression respond to cetuximab therapy. Sci Rep 2013; 3:2992.

[0230]   22. Teicher B A. Tumor models for preclinical development of targeted agents. Progress in drug research Fortschritte der Arzneimittelforschung Progres des recherches pharmaceutiques 2005; 63:43-66.

[0231]   23. Therasse P, Arbuck S G, Eisenhauer E A, Wanders J, Kaplan R S, Rubinstein L, et al. New guidelines to evaluate the response to treatment in solid tumors. European Organization for Research and Treatment of Cancer, National Cancer Institute of the United States, National Cancer Institute of Canada. J Natl Cancer Inst 2000; 92(3):205-16.

[0232]   24. Townsend E C, Murakami M A, Christodoulou A, Christie A L, Koster J, DeSouza T A, et al. The Public Repository of Xenografts Enables Discovery and Randomized Phase II-like Trials in Mice. Cancer cell 2016; 29(4):574-86.

[0233]   25. Heitjan D F, Manni A, Santen R J. Statistical analysis of in vivo tumor growth experiments. Cancer research 1993; 53(24):6042-50.

[0234]   26. Wu J. Statistical inference for tumor growth inhibition T/C ratio. Journal of biopharmaceutical statistics 2010; 20(5):954-64.

[0235]   27. Laajala T D, Corander J, Saarinen N M, Makela K, Savolainen S, Suominen M I, et al. Improved statistical modeling of tumor growth and treatment effect in preclinical animal studies with highly heterogeneous responses in vivo. Clinical cancer research: an official journal of the American Association for Cancer Research 2012; 18(16):4385-96.

[0236]   28. Zhao L, Morgan M A, Parsels L A, Maybaum J, Lawrence T S, Normolle D. Bayesian hierarchical changepoint methods in modeling the tumor growth profiles in xenograft experiments. Clinical cancer research: an official journal of the American Association for Cancer Research 2011; 17(5):1057-64.

14

[0237] 29. Xia C, Wu J, Liang H. Model Tumor Pattern and Compare Treatment Effects Using Semiparametric Linear Mixed-Effects Models. Journal of Biometrics & Biostatistics 2013

[0238] 30. Pierrillas P B, Tod M, Amiel M, Chenel M, Henin E. Improvement of Parameter Estimations in Tumor Growth Inhibition Models on Xenografted Animals: Handling Sacrifice Censoring and Error Caused by Experimental Measurement on Larger Tumor Sizes. The AAPS journal 2016.

[0239] 31. Choudhury K R, Kasman I, Plowman G D. Analysis of multi-arm tumor growth trials in xenograft animals using phase change adaptive piecewise quadratic models. Statistics in medicine 2010; 29(23):2399-409.

[0240] 32. Yang M, Shan B, Li Q, Song X, Cai J, Deng J, et al. Overcoming erlotinib resistance with tailored treatment regimen in patient-derived xenografts from naive Asian NSCLC patients. International journal of cancer Journal international du cancer 2013; 132(2):E74-84.

[0241] 33. Yang M, Xu X, Cai J, Ning J, Wery J P, Li Q X. NSCLC harboring EGFR exon-20 insertions after the regulatory C-helix of kinase domain responds poorly to known EGFR inhibitors. International journal of cancer Journal international du cancer 2016; 139(1):171-6.

[0242] 34. Hinkley D V. On the Ratio of Two Correlated Normal Random Variables. Biometrika 1969; 56(3):635-39.

[0243] 35. Brody J P, Williams B A, Wold B J, Quake S R. Significance and statistical errors in the analysis of DNA microarray data. Proceedings of the National Academy of Sciences of the United States of America 2002; 99(20): 12975-8.

[0244] 36. Zhang L, Yang J, Cai J, Song X, Deng J, Huang X, et al. A subset of gastric cancers with EGFR amplification and overexpression respond to cetuximab therapy. Scientific reports 2013; 3:2992.

[0245] 37. Kumar P, Henikoff S, Ng PC. Predicting the effects of coding non-synonymous variants on protein function using the SIFT algorithm. Nature protocols 2009; 4(7): 1073-81.

[0246] 38. Zhang X, Xu J, Liu H, Yang L, Liang J, Xu N, et al. Predictive biomarkers for the efficacy of cetuximab combined with cisplatin and capecitabine in advanced gastric or esophagogastric junction adenocarcinoma: a prospective multicenter phase 2 trial. Medical oncology 2014; 31(10):226.

[0247] 39. West B T, Welch K B, Galecki A T. Linear Mixed Models: A Practical Guide Using Statistical Software, Second Edition. Crc Press 2014.

[0248] 40. De Dosso S, Zanellato E, Nucifora M, Boldorini R, Sonzogni A, Biffi R, et al. ERCC1 predicts outcome in patients with gastric cancer treated with adjuvant cisplatin-based chemotherapy. Cancer chemotherapy and pharmacology 2013; 72(1):159-65.

[0249] 41. Wang J, Zhou X Q, Li J Y, Cheng J F, Zeng X N, Li X, et al. Prognostic significance of ERCC1 expression in postoperative patients with gastric cancer. Chinese journal of cancer research=Chung-kuo yen cheng yen chiu 2014; 26(3):323-30.

[0250] 42. Metzger R, Leichman C G, Danenberg K D, Danenberg P V, Lenz H J, Hayashi K, et al. ERCC1 mRNA levels complement thymidylate synthase mRNA levels in predicting response and survival for gastric cancer patients receiving combination cisplatin and fluorouracil chemotherapy. Journal of clinical oncology: official journal of the American Society of Clinical Oncology 1998; 16(1):309-16.

[0251] 43. Kwon H C, Roh M S, Oh S Y, Kim S H, Kim M C, Kim J S, et al. Prognostic value of expression of ERCC1, thymidylate synthase, and glutathione S-transferase P1 for 5-fluorouracil/oxaliplatin chemotherapy in advanced gastric cancer. Annals of oncology: official journal of the European Society for Medical Oncology/ ESMO 2007; 18(3):504-9.

[0252] 44. Hirakawa M, Sato Y, Ohnuma H, Takayama T, Sagawa T, Nobuoka T, et al. A phase II study of neoadjuvant combination chemotherapy with docetaxel, cisplatin, and S-1 for locally advanced resectable gastric cancer: nucleotide excision repair (NER) as potential chemoresistance marker. Cancer chemotherapy and pharmacology 2013; 71(3):789-97.

[0253] 45. Miura J T, Xiu J, Thomas J, George B, Carron B R, Tsai S, et al. Tumor profiling of gastric and esophageal carcinoma reveal different treatment options. Cancer biology & therapy 2015; 16(5):764-9.

[0254] 46. Bamias A, Karina M, Papakostas P, Kostopoulos I, Bobos M, Vourli G, et al. A randomized phase III study of adjuvant platinum/docetaxel chemotherapy with or without radiation therapy in patients with gastric cancer. Cancer Chemotherapy & Pharmacology 2010; 65(6): 1009-21.

[0255] 47. Baek S K, Kim S Y, Lee J J, Kim Y W, Yoon H J, Cho K S. Increased ERCC expression correlates with improved outcome of patients treated with cisplatin as an adjuvant therapy for curatively resected gastric cancer. Cancer Research & Treatment 2006; 38(1):19-24.

[0256] 48. Kim K H, Kwon H C, Oh S Y, Kim S H, Lee S, Kwon K A, et al. Clinicopathologic significance of ERCC1, thymidylate synthase and glutathione S-transferase P1 expression for advanced gastric cancer patients receiving adjuvant 5-FU and cisplatin chemotherapy. Biomarkers: biochemical indicators of exposure, response, and susceptibility to chemicals 2011; 16(1):74-82.

[0257] 49. Sonnenblick A, Rottenberg Y, Kadouri L, Wygoda M, Rivkind A, Vainer G W, et al. Long-term outcome of continuous 5-fluorouracil/cisplatin-based chemotherapy followed by chemoradiation in patients with resected gastric cancer. Medical oncology 2012; 29(5): 3035-8.

[0258] 50. Squires M H, 3rd, Fisher S B, Fisher K E, Patel S H, Kooby D A, El-Rayes B F, et al. Differential expression and prognostic value of ERCC1 and thymidylate synthase in resected gastric adenocarcinoma. Cancer 2013; 119(17):3242-50.

[0259] 51. Rondeau V, Mazroui Y, Gonzalez J R. frailtypack: An R Package for the Analysis of Correlated Survival Data with Frailty Models Using Penalized Likelihood Estimation or Parametrical Estimation. Journal of Statistical Software 2012; 47(4):1-28.

[0260] 52. Hanagal D D. Modeling survival data using frailty models. Statistical Methods in Medical Research 2015; 24(6):936-36.

[0261] 53. Benzekry S, Lamont C, Beheshti A, Tracz A, Ebos J M, Hlatky L, et al. Classical mathematical models for description and prediction of experimental tumor growth. PLoS computational biology 2014; 10(8): e1003800.

[0262] 54. Ferrer L, Rondeau V, Dignam J, Pickles T, Jacqmin-Gadda H, Proust-Lima C. Joint modelling of longitudinal and multi-state processes: application to clinical progressions in prostate cancer. Statistics in medicine 2016.

What is claimed is:

1. A method of conducting mouse clinical trial comprising the steps of:

receiving a dataset of tumor volumes measured in a mouse clinical trial, wherein the mouse clinical trial comprises the steps of:

obtaining a tumor sample derived from a patient;

grafting the tumor sample to a treatment group comprising m mice and a control group comprising n mice, wherein m and n are integers;

administering a drug to the treatment group;

administering a vehicle to the control group; and

measuring tumor volume of the treatment group and tumor volume of the control group at a plurality of days;

determining tumor growth curve of the treatment group and tumor growth curve of the control group;

determining area under curve (AUC) of the treatment group (AUC_T) and AUC of the control group (AUC_C); and

evaluating efficacy of the drug based on an AUC ratio between the AUC_T and the AUC_C.

2. The method of claim 1,

wherein the $AUC_T = \int_0^{d(T)} \ln V_x^{(T)} dx - d(T) \times \ln V_0^{(T)}$,

wherein $V_0^{(T)}$ is the tumor volume of the treatment group at day 0, $V_x^{(T)}$ is the tumor volume of the treatment group at day x, d(T) is the number of days the measuring step for the treatment group lasts; and

wherein the $AUC_C = \int_0^d \ln V_x^{(C)} dx - d \times \ln V_0^{(C)}$,

wherein $V_0(C)$ is the tumor volume of the control group at day 0, $V_x^{(C)}$ is the tumor volume of the control group at day x, d(C) is the number of days the measuring step for the treatment group lasts.

3. The method of claim 2, wherein d(T)=d(C), wherein the

$$AUC \text{ ratio} = \frac{AUC_T}{AUC_C}.$$

4. The method of claim 2, wherein d(T)≠d(C), wherein the

$$AUC \text{ ratio} = \frac{AUC_T / d(T)^2}{AUC_C / d(C)^2}.$$

5. The method of claim 1, wherein m≥3 and n≥3.

6. The method of claim 1, wherein m=n.

7. The method of claim 1, wherein the evaluating step comprises determining that the drug is effective when the AUC ratio is less than 1.

8. The method of claim 1, further comprising the step of determining correlation of a factor to the efficacy of the drug.

9. The method of claim 8, wherein the factor is expression level of a gene.

10. The method of claim 9, wherein the gene is EGFR and the drug is cetuximab.

11. The method of claim 1, wherein the tumor volumes are between 100-300 mm^3.

12. A method of conducting mouse clinical trial comprising the steps of:

receiving a dataset of tumor volumes measured in a mouse clinical trial, wherein the mouse clinical trial comprises the steps of:

obtaining a tumor sample derived from a patient;

grafting the tumor sample to a treatment group comprising m mice and a control group comprising n mice, wherein m and n are integers;

administering a drug to the treatment group;

administering a vehicle to the control group; and

measuring tumor volume of the treatment group and tumor volume of the control group at a plurality of days;

evaluating impact of a factor on the tumor volume of the treatment group, wherein the tumor volume of the treatment group after logarithmic transformation has a linear relationship with the factor.

13. The method of claim 12, wherein the factor is selected from the group consisting of:

efficacy of the drug, cancer type of the patient, expression level of a gene, and existence of a mutation.

14. The method of claim 13, wherein the drug is cisplatin.

15. The method of claim 14, wherein the cancer type is esophageal cancer, gastric cancer or lung cancer.

16. The method of claim 13, wherein the gene is ERCC.

17. The method of claim 12, wherein m≥3 and n≥3.

18. The method of claim 12, wherein m=n.

19. The method of claim 12, further comprising conducting a second mouse clinical trial based on the impact of the factor determined in the evaluation step.

20. A method of conducting a mouse clinical trial, comprising

receiving a dataset of tumor volumes in a mouse clinical trial, wherein the mouse clinical trial comprises the steps of:

obtaining a plurality of tumor samples derived from a plurality of patients;

grafting the plurality of tumor samples to a treatment group of mice and a control group of mice;

administering a drug to the treatment group;

administering a vehicle to the control group; and

measuring tumor volume of the treatment group and tumor volume of the control group at a plurality of days;

determining progress-free survival (PFS) or overall survival (OS) of the treatment group and the control group;

evaluating efficacy of the drug based on the PFS or OS using an additive frailty model.

21. The method of claim 20, wherein the additive frailty model includes a hazard function, wherein the hazard function for the j-th mouse of the i-th PDX is

$$h_{ij}(t) = h_0(t) \exp(u_i + (w + v_i)T_{ij} + \beta^T X_i)$$

wherein h_0 (t) is a baseline hazard function, u_i is a random effect associated with the i-th patient without drug treatment, w is mean drug effect, v_i is a random effect associated the i-th patient that depicts drug response deviating from w, T_{ij} is 0 for the control group and 1 for the treatment group, X_i is a vector for a covariate of the plurality of patients, β^T is a vector quantifying fixed effects of the covariate.

22. The method of claim 20, wherein the PFS is the time until the tumor volume doubles.

23. The method of claim **21**, wherein the covariate is cancer type, expression of a gene or a gene mutation.

24. The method of claim **20**, wherein the treatment group consists of n mice for each patient and the control group consists of n mice for each patient, wherein n≥3.

25. The method of claim **21**, further comprising conducting a second mouse clinical trial based on the hazard function.

* * * * *